



A model-independent analysis of $b \rightarrow s \mu^+ \mu^-$ transitions with GAMBIT's FlavBit

Jihyun Bohm^{1,a}, Marcin Chrzaszcz^{1,b}, Farvah Mahmoudi^{2,3,c}, Markus T. Prim⁴, Pat Scott^{5,6}, Martin White⁷

¹ Henryk Niewodniczanski Institute of Nuclear Physics Polish Academy of Sciences, Kraków, Poland

² Univ Lyon, Univ Lyon 1, CNRS/IN2P3, Institut de Physique Nucléaire de Lyon, UMR5822, 69622 Villeurbanne, France

³ Theoretical Physics Department, CERN, 1211 Geneva 23, Switzerland

⁴ Institute of Experimental Particle Physics, Karlsruhe Institute of Technology, Karlsruhe, Germany

⁵ School of Mathematics and Physics, The University of Queensland, St. Lucia, Brisbane, QLD 4072, Australia

⁶ Department of Physics, Imperial College London, South Kensington SW7 2AZ, UK

⁷ Department of Physics, University of Adelaide, Adelaide, SA 5005, Australia

Received: 26 May 2021 / Accepted: 17 November 2021

© The Author(s) 2021

Abstract The search for flavour-changing neutral current effects in B -meson decays is a powerful probe of physics beyond the Standard Model. Deviations from SM behaviour are often quantified by extracting the preferred values of the Wilson coefficients of an operator product expansion. We use the FlavBit module of the GAMBIT package to perform a simultaneous global fit of the Wilson coefficients C_7 , C_9 , and C_{10} using a combination of all current data on $b \rightarrow s \mu^+ \mu^-$ transitions. We further extend previous analyses by accounting for the correlated theoretical uncertainties at each point in the Wilson coefficient parameter space, rather than deriving the uncertainties from a Standard Model calculation. We find that the best fit deviates from the SM value with a significance of 6.6σ . The largest deviation is associated with a vector coupling of muons to b and s quarks.

1 Introduction

In the Standard Model (SM), flavour-changing neutral currents (FCNC) are heavily suppressed by the Glashow–Iliopoulos–Maiani (GIM; [1]) mechanism. Since the start of the LHC, experiments have observed numerous deviations from the predictions of the SM in $b \rightarrow s \mu^+ \mu^-$ transitions, starting with the 2013 LHCb collaboration observation of a deviation in the P_5' observable in the range $q^2 \in [4.30, 8.68]$ GeV²/c⁴ of the decay $B_d \rightarrow K^{*0} \mu^+ \mu^-$ [2]. Further discrepancies were later observed in measurements of the $B_s \rightarrow \phi \mu^+ \mu^-$ [3,4], $B \rightarrow K \mu^+ \mu^-$ [5], and $\Lambda_b \rightarrow$

$\Lambda \mu^+ \mu^-$ [6] decays in both the angular and branching fraction observables. Given the consistency of the observations, other experiments [7–9] have performed measurements of the $B_d \rightarrow K^{*0} \mu^+ \mu^-$ decay, finding results consistent with the discrepancies seen earlier.

As has been studied in previous analyses, the discrepancies can be solved by reducing the C_9 Wilson coefficient by one quarter of the SM value (see for example Refs. [10–20]). Unfortunately, these processes suffer from non-factorisable corrections, making the size of the theoretical uncertainties, and therefore the overall significance of the results, difficult to quantify (see Refs. [21–28] for a recent discussion of the hadronic corrections).

The SM predicts that the rate of $b \rightarrow s \ell \ell$ transitions is independent of the flavour of the leptons involved, except for mass effects which are negligible when studying the first two generations $\ell = e, \mu$. In addition to the discrepancies seen purely with muons, the LHCb collaboration has therefore also performed explicit tests of lepton universality in $b \rightarrow s \ell \ell$ transitions. The first test is to measure the ratio $R_K \equiv \mathcal{B}(B \rightarrow K \mu^+ \mu^-) / \mathcal{B}(B_d \rightarrow K e^+ e^-)$, whilst a second is to measure $R_{K^*} = \mathcal{B}(B_d \rightarrow K^{*0} \mu^+ \mu^-) / \mathcal{B}(B_d \rightarrow K^{*0} e^+ e^-)$. In both cases the SM prediction is known at the 1% level, as the hadronic uncertainties cancel in taking the ratio of the two branching ratios. The LHCb experiment measured a lower value than the SM prediction with a significance of 3.1σ and 2.1 – 2.5σ for R_K and R_{K^*} respectively [29,30].

In this paper, we focus mainly on tests with muons, exploring the extent to which the combination of all such data to date either constrain flavour-universal new physics (i.e. coupling identically to all leptons) in $b \rightarrow s$ transitions, or prefer it in comparison to the SM. Using the FlavBit [31] module of the Global and Modular Beyond-Standard Model Inference

^a e-mail: jihyun.bohm@cern.ch (corresponding author)

^b e-mail: marcin.chrzaszcz@cern.ch (corresponding author)

^c e-mail: mahmoudi@in2p3.fr (corresponding author)

Tool (GAMBIT; [32,33]), we carry out a model-independent analysis by simultaneously fitting three Wilson coefficients in an effective field theory for interactions of b and s quarks with leptons and photons. We significantly improve on previous analyses by explicitly re-computing theory uncertainties at every Wilson coefficient combination, rather than assuming that they are constant and given by their SM values across the entire parameter space. The final result is a 6.6σ preference for new physics, overwhelmingly associated with the vector coupling of muons to b and s quarks.

We begin in Sect. 2 with a description of the effective field theory framework in which we work, followed by explanations of the observables (Sect. 3) and likelihoods (Sect. 4) involved in our fits. We show the results of our analysis in Sect. 5, including preferred regions of the Wilson coefficient parameter space and the spectrum of observables at our best-fit point, before concluding in Sect. 6.

2 Theoretical framework

Our analysis is based on the effective Hamiltonian approach, in which the Operator Product Expansion is used to separate physics at low energies from a (possibly unknown) high energy theory. In this framework, the transition from an initial state i to a final state f is proportional to the squared matrix element $|\langle f | \mathcal{H}_{\text{eff}} | i \rangle|^2$, with the effective Hamiltonian for $b \rightarrow s$ transitions given by

$$\mathcal{H}_{\text{eff}} = -\frac{4G_F}{\sqrt{2}} V_{tb} V_{ts}^* \sum_{i=1}^{10} \left(C_i(\mu) \mathcal{O}_i(\mu) + C'_i(\mu) \mathcal{O}'_i(\mu) \right). \tag{2.1}$$

G_F , V_{tb} and V_{ts} are SM parameters (the Fermi constant and two CKM matrix elements, respectively), μ is the energy scale at which the calculation is being performed, and the \mathcal{O}_i are local operators providing low-energy descriptions of high-energy physics that has been integrated out. The operators each come with an associated Wilson coefficient C_i which, for a particular high-energy physics model, is calculable within the framework of perturbation theory. This is done by matching the high-scale theory to the low-energy effective theory at a scale μ_W , which is of the order of the W boson mass. The renormalisation group equations of the low-energy effective theory can then be used to evolve the Wilson coefficients to the scale μ_b , which characterises B meson decay calculations and is thus of order m_b .

The operators that are most relevant for rare B decays featuring FCNCs are

$$\begin{aligned} \mathcal{O}_1 &= (\bar{s}\gamma_\mu T^a P_L c)(\bar{c}\gamma^\mu T^a P_L b), \\ \mathcal{O}_2 &= (\bar{s}\gamma_\mu P_L c)(\bar{c}\gamma^\mu P_L b), \end{aligned}$$

$$\begin{aligned} \mathcal{O}_3 &= (\bar{s}\gamma_\mu P_L b) \sum_q (\bar{q}\gamma^\mu q), \\ \mathcal{O}_4 &= (\bar{s}\gamma_\mu T^a P_L b) \sum_q (\bar{q}\gamma^\mu T^a q), \\ \mathcal{O}_5 &= (\bar{s}\gamma_{\mu_1}\gamma_{\mu_2}\gamma_{\mu_3} P_L b) \sum_q (\bar{q}\gamma^{\mu_1}\gamma^{\mu_2}\gamma^{\mu_3} q), \\ \mathcal{O}_6 &= (\bar{s}\gamma_{\mu_1}\gamma_{\mu_2}\gamma_{\mu_3} T^a P_L b) \sum_q (\bar{q}\gamma^{\mu_1}\gamma^{\mu_2}\gamma^{\mu_3} T^a q), \\ \mathcal{O}_7 &= \frac{e}{(4\pi)^2} m_b (\bar{s}\sigma^{\mu\nu} P_R b) F_{\mu\nu}, \\ \mathcal{O}_8 &= \frac{g}{(4\pi)^2} m_b (\bar{s}\sigma^{\mu\nu} T^a P_R b) G_{\mu\nu}^a, \\ \mathcal{O}_9 &= \frac{e^2}{(4\pi)^2} (\bar{s}\gamma^\mu P_L b)(\bar{\ell}\gamma_\mu \ell), \\ \mathcal{O}_{10} &= \frac{e^2}{(4\pi)^2} (\bar{s}\gamma^\mu P_L b)(\bar{\ell}\gamma_\mu \gamma_5 \ell). \end{aligned} \tag{2.2}$$

The same set of operators applies for $b \rightarrow d$ processes, with the valence strange quark substituted by a valence down quark. We have denoted the b -quark mass by m_b , the strong coupling by g , the $SU(3)_c$ generators by T^a , and the photon and gluon field-strength tensors by $F_{\mu\nu}$ and $G_{\mu\nu}^a$. The sums run over the relevant quark flavours $q = u, d, s, c, b$.

Global statistical fits of the Wilson coefficients with flavour physics data are a standard way to uncover evidence for possible beyond-SM (BSM) physics contributions, in a way that remains agnostic to the precise high-scale theory that supersedes the SM.

In our analysis we allow for modification of three Wilson coefficients:

$$\begin{aligned} C_7 &= C_7^{\text{SM}} + \Delta C_7, \\ C_9 &= C_9^{\text{SM}} + \Delta C_9, \\ C_{10} &= C_{10}^{\text{SM}} + \Delta C_{10}, \end{aligned}$$

where C_i^{SM} is the SM value of the i th Wilson coefficient ($\text{Re}(C_{7,9,10}^{\text{SM}}) = -0.29, 4.20, -4.06$), whereas ΔC_i is its modification by some high-energy new physics. In the fit that we perform in this paper, we vary the real parts of ΔC_7 , ΔC_9 and ΔC_{10} to best match the experimental results.

3 Observables included in the fit

In this section we will discuss the theoretical calculations of the observables that are included in the fit. We perform the calculations with the latest version of FlavBit [31], which uses SuperIso 4.1 [34–36]. Below, we provide a brief description for completeness.

3.1 Angular distribution and branching fraction of $B_d \rightarrow K^*0 \mu^+ \mu^-$ decays

The decay $B_d \rightarrow K^*0 \mu^+ \mu^-$ is of particular interest as it presents a wide variety of experimentally-accessible observables. On the other hand, in general the hadronic uncertainties in the theoretical predictions are large. The decay with K^* on the mass shell has a fourfold differential distribution

$$\frac{d^4\Gamma[B_d \rightarrow K^*0(\rightarrow K\pi)\mu^+\mu^-]}{dq^2 d\cos\theta_l, d\cos\theta_K d\phi} = \frac{9}{32\pi} \sum_i J_i(q^2) g_i(\theta_l, \theta_K, \phi), \tag{3.1}$$

with respect to the three angles θ_l, θ_K , and ϕ (as defined in [37]) and the dilepton invariant mass q^2 . In the low- q^2 region (where q^2 is below the J/ψ resonance), the description of this decay is provided by the method of QCD-improved factorisation (QCDF) and the Soft-Collinear Effective Theory (SCET).

The functions J_{1-9} can be written in terms of the transversity amplitudes, $A_0, A_{\parallel}, A_{\perp}, A_t$ (and A_S if scalar operators are also considered and lepton mass is not neglected) [38]:

$$J_1^S = \frac{(2 + \beta_\ell^2)}{4} \left[|A_{\perp}^L|^2 + |A_{\parallel}^L|^2 + (L \rightarrow R) \right] + \frac{4m_\ell^2}{q^2} \text{Re} \left(A_{\perp}^L A_{\perp}^{R*} + A_{\parallel}^L A_{\parallel}^{R*} \right), \tag{3.2a}$$

$$J_1^C = |A_0^L|^2 + |A_0^R|^2 + \frac{4m_\ell^2}{q^2} \left[|A_t|^2 + 2\text{Re}(A_0^L A_0^{R*}) \right] + \beta_\ell^2 |A_S|^2, \tag{3.2b}$$

$$J_2^S = \frac{\beta_\ell^2}{4} \left[|A_{\perp}^L|^2 + |A_{\parallel}^L|^2 + (L \rightarrow R) \right], \tag{3.2c}$$

$$J_2^C = -\beta_\ell^2 \left[|A_0^L|^2 + (L \rightarrow R) \right], \tag{3.2d}$$

$$J_3 = \frac{1}{2} \beta_\ell^2 \left[|A_{\perp}^L|^2 - |A_{\parallel}^L|^2 + (L \rightarrow R) \right], \tag{3.2e}$$

$$J_4 = \frac{1}{\sqrt{2}} \beta_\ell^2 \left[\text{Re}(A_0^L A_{\parallel}^{L*}) + (L \rightarrow R) \right], \tag{3.2f}$$

$$J_5 = \sqrt{2} \beta_\ell \left[\text{Re}(A_0^L A_{\perp}^{L*}) - (L \rightarrow R) - \frac{m_\ell}{\sqrt{q^2}} \text{Re}(A_{\parallel}^L A_S^{R*} + A_{\parallel}^R A_S^{L*}) \right], \tag{3.2g}$$

$$J_6^S = 2\beta_\ell \left[\text{Re}(A_{\parallel}^L A_{\perp}^{L*}) - (L \rightarrow R) \right], \tag{3.2h}$$

$$J_6^C = 4\beta_\ell \frac{m_\ell}{\sqrt{q^2}} \text{Re} \left[A_0^L A_S^{R*} + (L \rightarrow R) \right], \tag{3.2i}$$

$$J_7 = \sqrt{2} \beta_\ell \left[\text{Im}(A_0^L A_{\parallel}^{L*}) - (L \rightarrow R) + \frac{m_\ell}{\sqrt{q^2}} \text{Im}(A_{\perp}^L A_S^{R*} + A_{\perp}^R A_S^{L*}) \right], \tag{3.2j}$$

$$J_8 = \frac{1}{\sqrt{2}} \beta_\ell^2 \left[\text{Im}(A_0^L A_{\perp}^{L*}) + (L \rightarrow R) \right], \tag{3.2k}$$

$$J_9 = \beta_\ell^2 \left[\text{Im}(A_{\parallel}^L A_{\perp}^{L*}) + (L \rightarrow R) \right], \tag{3.2l}$$

where $\beta_\ell \equiv \sqrt{1 - 4m_\ell^2/q^2}$ and $(L \rightarrow R)$ indicates the same terms as immediately preceding, but with L and R superscripts exchanged.

The transversity amplitudes are related to the Wilson coefficients and form factors as

$$A_{\perp}^{L,R} = N \sqrt{2\lambda} \left[(C_9 + Y(q^2) + C_9') \mp (C_{10} + C_{10}') \right] \times \frac{V(q^2)}{M_B + M_V} + \frac{2m_b}{q^2} (C_7^{\text{eff}} + C_7') T_1(q^2), \tag{3.3}$$

$$A_{\parallel}^{L,R} = -N \sqrt{2}(M_B^2 - M_V^2) \times \left[(C_9 + Y(q^2) - C_9') \mp (C_{10} - C_{10}') \right] \frac{A_1(q^2)}{M_B - M_V} + \frac{2m_b}{q^2} (C_7^{\text{eff}} - C_7') T_2(q^2), \tag{3.4}$$

$$A_0^{L,R} = -\frac{N}{2M_V \sqrt{q^2}} \left\{ \left[(C_9 + Y(q^2) - C_9') \mp (C_{10} - C_{10}') \right] \times \left[(M_B^2 - M_V^2 - q^2)(M_B + M_V) A_1(q^2) - \lambda \frac{A_2(q^2)}{M_B + M_V} \right] + 2m_b(C_7^{\text{eff}} - C_7') \times \left[(M_B^2 + 3M_V^2 - q^2) T_2(q^2) - \frac{\lambda}{M_B^2 - M_V^2} T_3(q^2) \right] \right\}, \tag{3.5}$$

$$A_t = \frac{N}{\sqrt{q^2}} \sqrt{\lambda} \left[2(C_{10} - C_{10}') + \frac{q^2}{m_\ell(m_b + m_q)} (C_{Q_2} - C_{Q_2}') \right] A_0(q^2), \tag{3.6}$$

$$A_S = -\frac{2N}{m_b + m_q} \sqrt{\lambda} (C_{Q_1} - C_{Q_1}') A_0(q^2), \tag{3.7}$$

where M_V is the K^* (vector) meson mass, m_q the spectator quark mass and

$$N = V_{tb} V_{ts}^* \left[\frac{G_F^2 \alpha^2}{3 \cdot 2^{10} \pi^5 M_B^3} q^2 \beta_\ell \sqrt{\lambda(M_B^2, M_V^2, q^2)} \right]^{1/2}, \tag{3.8}$$

with the Källén function

$$\lambda(x, y, z) \equiv x^2 + y^2 + z^2 - 2(xy + yz + xz). \tag{3.9}$$

C_7^{eff} is defined as

$$C_7^{\text{eff}} = C_7(\mu) - \frac{1}{3}C_3(\mu) - \frac{4}{9}C_4(\mu) - \frac{20}{3}C_5(\mu) - \frac{80}{9}C_6(\mu), \tag{3.10}$$

and the function $Y(q^2)$ is given by

$$Y(q^2) = h(q^2, m_c) \left(\frac{4}{3}C_1 + C_2 + 6C_3 + 60C_5 \right) - \frac{1}{2}h(q^2, m_b^{\text{pole}}) \left(7C_3 + \frac{4}{3}C_4 + 76C_5 + \frac{64}{3}C_6 \right) - \frac{1}{2}h(q^2, 0) \left(C_3 + \frac{4}{3}C_4 + 16C_5 + \frac{64}{3}C_6 \right) + \frac{4}{3}C_3 + \frac{64}{9}C_5 + \frac{64}{27}C_6, \tag{3.11}$$

with

$$h(q^2, m_q) = -\frac{4}{9} \left(\ln \frac{m_q^2}{\mu^2} - \frac{2}{3} - z \right) - \frac{4}{9} (2+z)\sqrt{|z-1|} \times \begin{cases} \arctan \frac{1}{\sqrt{z-1}} & z > 1 \\ \ln \frac{1+\sqrt{1-z}}{\sqrt{z}} - \frac{i\pi}{2} & z \leq 1 \end{cases} \tag{3.12}$$

where $z = 4m_q^2/q^2$. For the form factors $A_{1,2,3}(q^2)$, $V(q^2)$, $T_{1,2,3}(q^2)$ we use the combined LCSR + lattice results from Ref. [39]. The precise values of these form factors are correlated, and together depend on 21 nuisance parameters. When obtaining the correlation matrix between the theoretical uncertainties on the different observables that enter our fit, we include these parameters in our marginalisation over theoretical uncertainties using Monte Carlo methods in SuperIso 4.1, for each combination of Wilson coefficients.

In addition, the transversity amplitudes receive corrections arising from the hadronic part of the Hamiltonian, through the emission of a photon which itself turns into a lepton pair. The leading contributions at low q^2 can be calculated within the QCD factorisation approach where an expansion of Λ/m_b is employed, but the subleading nonfactorisable power corrections are difficult to estimate. The corrections to the transversity amplitudes can be written as

$$\delta A_{\perp}^{L,R} = \frac{32\pi^2 N m_B^3}{\sqrt{2} q^2} \left(\mathcal{N}_+(q^2) - \mathcal{N}_-(q^2) \right), \tag{3.13}$$

$$\delta A_{\parallel}^{L,R} = \frac{32\pi^2 N m_B^3}{\sqrt{2} q^2} \left(\mathcal{N}_+(q^2) + \mathcal{N}_-(q^2) \right), \tag{3.14}$$

$$\delta A_0^{L,R} = \frac{32\pi^2 N m_B^3}{q^2} \left(\mathcal{N}_0(q^2) \right). \tag{3.15}$$

The QCdf contributions to $\mathcal{N}_{\lambda}(q^2)$ are

$$\mathcal{N}_{\pm}^{\text{QCdf}} = -\frac{1}{16\pi^2} \frac{m_b}{m_B} \left[(m_B^2 - m_V^2) \frac{2E_V}{m_B^3} \left(\mathcal{T}_{\perp}^{-(t),\text{nf+WA}} + \hat{\lambda}_u \mathcal{T}_{\perp}^{-(u)} \right) \mp \frac{\sqrt{\lambda}}{m_B^2} \left(\mathcal{T}_{\perp}^{+(t),\text{nf+WA}} + \hat{\lambda}_u \mathcal{T}_{\perp}^{+(u)} \right) \right], \tag{3.16}$$

$$\mathcal{N}_0^{\text{QCdf}} = -\frac{1}{16\pi^2} \frac{m_b}{m_B} \frac{\sqrt{q^2}}{2m_V} \times \left\{ \left[(m_B^2 + 3m_V^2 - q^2) \frac{2E_V}{m_B^3} - \frac{\lambda}{(m_B^2 - m_V^2)m_B^2} \right] \times \left(\mathcal{T}_{\perp}^{-(t),\text{nf+WA}} + \hat{\lambda}_u \mathcal{T}_{\perp}^{-(u)} \right) - \frac{\lambda}{(m_B^2 - m_V^2)m_B^2} \left(\mathcal{T}_{\parallel}^{-(t),\text{nf+WA}} + \hat{\lambda}_u \mathcal{T}_{\parallel}^{-(u)} \right) \right\}, \tag{3.17}$$

where $\hat{\lambda}_u = (V_{ub}V_{us}^*)/(V_{tb}V_{ts}^*)$ and the expressions for \mathcal{T}^{\pm} can be found in Ref. [40]. The remaining hadronic corrections are unknown, and are assumed to be a fraction of the leading order non-factorisable contribution. They can be parameterised by multiplying $Y(q^2)$ and the $\delta A_{\lambda}^{L,R}$ by

$$\left[1 + a_{\lambda}^{L,R} + b_{\lambda}^{L,R} \left(\frac{q^2}{6 \text{ GeV}^2/c^4} \right) \right], \tag{3.18}$$

where $a_{\lambda}^{L,R}$ and $b_{\lambda}^{L,R}$ are taken as uncorrelated complex nuisance parameters. We model the distributions of their amplitudes as Gaussians centered at 0, with variances of 10% and 25% respectively in the low- q^2 region. In the high q^2 region, we assign a variance of 10% to the distribution of the amplitude of $a_{\lambda}^{L,R}$, and neglect the term proportional to $b_{\lambda}^{L,R}$, as in this regime the relative variation of q^2 is small compared to its variation at low q^2 , so one can neglect higher orders in the q^2 expansion (and the sensitivity to New Physics at high q^2 is very small anyway). The phases are unknown constants (see Refs. [41,42] for more details).

The traditional set of observables used to probe $B_d \rightarrow K^{*0} \mu^+ \mu^-$ decays consists of the differential branching fraction

$$\frac{d\Gamma}{dq^2} = \frac{3}{4} \left(J_1 - \frac{J_2}{3} \right), \tag{3.19}$$

where $J_i \equiv 2J_i^s + J_i^c$, and the angular observables

$$F_L(q^2) \equiv \frac{|A_0|^2}{|A_0|^2 + |A_{\parallel}|^2 + |A_{\perp}|^2}, \tag{3.20}$$

$$A_{\text{FB}}(q^2) \equiv \int_{-1}^0 d \cos \theta_l \frac{d^2\Gamma}{dq^2 d \cos \theta_l} \Big/ \frac{d\Gamma}{dq^2} - \int_0^1 d \cos \theta_l \frac{d^2\Gamma}{dq^2 d \cos \theta_l} \Big/ \frac{d\Gamma}{dq^2} = \frac{3}{8} J_6 \Big/ \frac{d\Gamma}{dq^2}. \tag{3.21}$$

In order to minimise the hadronic uncertainties emerging from form factor contributions to the $B_d \rightarrow K^{*0} \mu^+ \mu^-$ decay, angular observables have been constructed offering specific form-factor-independent observables (at leading order) [37, 38, 43, 44]. One such set of observables is the so-called *optimised observable set*, P'_i , defined as

$$\begin{aligned} \langle P_1 \rangle_{\text{bin}} &= \frac{1}{2} \frac{\int_{\text{bin}} dq^2 [J_3 + \bar{J}_3]}{\int_{\text{bin}} dq^2 [J_{2s} + \bar{J}_{2s}]}, \\ \langle P_2 \rangle_{\text{bin}} &= \frac{1}{8} \frac{\int_{\text{bin}} dq^2 [J_{6s} + \bar{J}_{6s}]}{\int_{\text{bin}} dq^2 [J_{2s} + \bar{J}_{2s}]}, \\ \langle P'_4 \rangle_{\text{bin}} &= \frac{1}{\mathcal{N}'_{\text{bin}}} \int_{\text{bin}} dq^2 [J_4 + \bar{J}_4], \\ \langle P'_5 \rangle_{\text{bin}} &= \frac{1}{2\mathcal{N}'_{\text{bin}}} \int_{\text{bin}} dq^2 [J_5 + \bar{J}_5], \\ \langle P'_6 \rangle_{\text{bin}} &= \frac{-1}{2\mathcal{N}'_{\text{bin}}} \int_{\text{bin}} dq^2 [J_7 + \bar{J}_7], \\ \langle P'_8 \rangle_{\text{bin}} &= \frac{-1}{\mathcal{N}'_{\text{bin}}} \int_{\text{bin}} dq^2 [J_8 + \bar{J}_8], \end{aligned} \tag{3.22}$$

where the normalisation $\mathcal{N}'_{\text{bin}}$ is given by

$$\mathcal{N}'_{\text{bin}} = \sqrt{-\int_{\text{bin}} dq^2 [J_{2s} + \bar{J}_{2s}] \int_{\text{bin}} dq^2 [J_{2c} + \bar{J}_{2c}]}. \tag{3.23}$$

Alternatively, one can define the observables [45–47]

$$S_i = \frac{J_{i(s,c)} + \bar{J}_{i(s,c)}}{\frac{d\Gamma}{dq^2} + \frac{d\bar{\Gamma}}{dq^2}}, \tag{3.24}$$

which are related to the P_i set as $S_i = P'_i \sqrt{F_L(1 - F_L)}$.

The most important measurements for the interpretation of $b \rightarrow s \mu^+ \mu^-$ transitions in terms of new physics are the angular observables in various q^2 bins of the $B_d \rightarrow K^{*0} \mu^+ \mu^-$ decay. They are currently measured by four collaborations: LHCb, Belle, ATLAS and CMS, with the most recent measurement being an LHCb analysis of part of the LHC Run II dataset [48]. In the case of this measurement, the whole set of angular observables is available with the full correlation matrix. In particular, LHCb provides angular observables in the S_i basis [45–47] as well as the so-called optimised observables [43]. The optimised observables are “clean” from hadronic uncertainties only at leading order, and with the current precision this is not enough for phenomenological applications. Furthermore, the optimised observables are non-linearly correlated with each other. In the following, we therefore use the measurements in the S_i basis. As was pointed out in [49], the conventional theoretical and experimental angular observables differ by a minus sign in the case of S_4, S_7 and S_9 , which we make sure to take into account.

The analyses of Belle [50], CMS [9] and ATLAS [8] include measurements of only a subset of the angular observables. This is due to the fact that their datasets contain a

smaller number of $B_d \rightarrow K^{*0} \mu^+ \mu^-$ decays than that of LHCb, so the full angular distributions cannot be determined without folding some of the angles [51]. In our fit, we use all observables for which measurements by Belle, CMS or ATLAS are currently available.

In addition to the angular observables, we use the measured branching fraction of the $B_d \rightarrow K^{*0} \mu^+ \mu^-$ decay in various q^2 bins. Currently the only measurement that distinguishes the s -wave and p -wave contributions is the LHCb one [52]. The theoretical framework discussed in Sect. 2 can only describe the p -wave contribution. It is therefore of crucial importance to take into account the branching fraction measurement that subtracts the s -wave contribution.

In addition to the $B_d \rightarrow K^{*0} \mu^+ \mu^-$ observables, we also include the corresponding observables from decays with electrons in our fit, i.e. $B_d \rightarrow K^{*0} e^+ e^-$.

3.2 Branching fraction of $B_s \rightarrow \phi \mu^+ \mu^-$ decays

The decay $B_s \rightarrow \phi \mu^+ \mu^-$ is also a $b \rightarrow s \mu^+ \mu^-$ transition, but with a valence strange quark. The decay has only currently been measured by the LHCb collaboration [53]. In contrast to the $B_d \rightarrow K^{*0} \mu^+ \mu^-$ decay, the $B_s \rightarrow \phi \mu^+ \mu^-$ decay is not self-tagging, and thus there is no experimental access to the most relevant CP -averaged observables S_i . Therefore, we use only the branching fraction information in our analysis. Because the ϕ meson has a much narrower width than the K^* meson, the s -wave pollution is negligible in this case.

The calculations for this decay are very similar to the ones for $B_d \rightarrow K^{*0} \mu^+ \mu^-$, with the main difference being that the spectator quark is a strange quark, and the meson masses and form factors are different. Here we use the form factors from the LCSR + lattice results [39].

Because the $B_s \rightarrow \phi \mu^+ \mu^-$ decay is not self-tagging, the untagged average over the \bar{B}_s and B_s decay distributions is required. Defining [54]

$$\tilde{J}_i = \zeta_i \bar{J}_i, \tag{3.25}$$

with

$$\begin{aligned} \zeta_i &= 1 \quad \text{for } i = 1s, 1c, 2s, 2c, 3, 4, 7; \\ \zeta_i &= -1 \quad \text{for } i = 5, 6s, 6c, 8, 9, \end{aligned} \tag{3.26}$$

and

$$x = \frac{\Delta M}{\Gamma}, \quad y = \frac{\Delta \Gamma}{2\Gamma}, \tag{3.27}$$

the averaged J_i functions are computed for LHCb with

$$\langle J_i + \bar{J}_i \rangle_{\text{Hadronic}} = \frac{1}{\Gamma} \left[\frac{J_i + \tilde{J}_i}{1 - y^2} - \frac{y h_j}{1 - y^2} \right], \tag{3.28}$$

and the time-dependent decay rate is given by

$$\left\langle \frac{d\Gamma}{dq^2} \right\rangle = \frac{1}{\Gamma(1-y^2)} \langle \mathcal{I} \rangle, \tag{3.29}$$

$$\begin{aligned} \langle \mathcal{I} \rangle_{\text{Hadronic}} &= \frac{3}{4} \left[2(J_{1s} + \bar{J}_{1s} - y h_{1s}) + (J_{1c} + \bar{J}_{1c} - y h_{1c}) \right] \\ &\quad - \frac{1}{4} \left[2(J_{2s} + \bar{J}_{2s} - y h_{2s}) + (J_{2c} + \bar{J}_{2c} - y h_{2c}) \right], \end{aligned} \tag{3.30}$$

where \mathcal{I} is the usual normalisation considered in analyses of the angular coefficients.

The coefficients h_i relevant for the decay rate are:

$$h_{1s} = \frac{2 + \beta_\ell^2}{2} \text{Re} \left[e^{i\phi} \left(\tilde{A}_\perp^L A_\perp^{L*} + \tilde{A}_\parallel^L A_\parallel^{L*} + \tilde{A}_\perp^R A_\perp^{R*} + \tilde{A}_\parallel^R A_\parallel^{R*} \right) \right] \tag{3.31}$$

$$\begin{aligned} &+ \frac{4m_\ell^2}{q^2} \text{Re} \left[e^{i\phi} \left(\tilde{A}_\perp^L A_\perp^{R*} + \tilde{A}_\parallel^L A_\parallel^{R*} \right) \right] \\ &+ e^{-i\phi} \left(A_\perp^L \tilde{A}_\perp^{R*} + A_\parallel^L \tilde{A}_\parallel^{R*} \right), \end{aligned} \tag{3.32}$$

$$\begin{aligned} h_{1c} &= 2\text{Re} \left[e^{i\phi} \left(\tilde{A}_0^L A_0^{L*} + \tilde{A}_0^R A_0^{R*} \right) \right] \\ &+ \frac{8m_\ell^2}{q^2} \left\{ \text{Re} \left[e^{i\phi} \tilde{A}_t A_t^* \right] \right. \\ &\quad \left. + \text{Re} \left[e^{i\phi} \tilde{A}_0^L A_0^{R*} + e^{-i\phi} A_0^L \tilde{A}_0^{R*} \right] \right\} + 2\beta_\ell^2 \text{Re} \left[e^{i\phi} \tilde{A}_S A_S^* \right], \end{aligned}$$

$$h_{2s} = \frac{\beta_\ell^2}{2} \text{Re} \left[e^{i\phi} \left(\tilde{A}_\perp^L A_\perp^{L*} + \tilde{A}_\parallel^L A_\parallel^{L*} + \tilde{A}_\perp^R A_\perp^{R*} + \tilde{A}_\parallel^R A_\parallel^{R*} \right) \right], \tag{3.33}$$

$$h_{2c} = -2\beta_\ell^2 \text{Re} \left[e^{i\phi} \left(\tilde{A}_0^L A_0^{L*} + \tilde{A}_0^R A_0^{R*} \right) \right], \tag{3.34}$$

where $\phi = 2\beta_s$, $\sin \phi = 0.04$, $x = 27$ and $y = 0.06$ [55]. The amplitudes \tilde{A}_X denote the amplitudes $A_X(\bar{B} \rightarrow f)$ in which CP-conjugation is not applied to the final state. The hadronic uncertainties due to power corrections are accounted for using Eq. (3.18).

3.3 Branching fraction of $B \rightarrow K \mu^+ \mu^-$ decays

Another member of the $b \rightarrow s \mu^+ \mu^-$ transition family is the decay $B \rightarrow K \mu^+ \mu^-$. Because the K is a scalar, the decay kinematics can be described with only one helicity angle, and the angular distribution has only two observables, which are in fact not sensitive to the Wilson coefficients that we consider here. We therefore consider only the branching fraction of the $B \rightarrow K \mu^+ \mu^-$ decay. The decay was measured by LHCb [56] and the B -factories Babar [57] and Belle [58]. In our fits, we only include data from LHCb, as the uncertainties of the B -factory measurements are more than a factor of 4 larger, and therefore do not contribute much to the global picture.

The $B \rightarrow K \ell \ell$ matrix element can be written as [59]

$$\begin{aligned} \mathcal{M}(B \rightarrow K \ell \ell) &= i \frac{G_F \alpha_e}{\sqrt{2}\pi} V_{tb} V_{ts}^* \\ &\times \left(F_V p_B^\mu [\bar{\ell} \gamma_\mu \ell] + F_A p_B^\mu [\bar{\ell} \gamma_\mu \gamma_5 \ell] \right. \\ &\quad \left. + (F_S + \cos \theta F_T) [\bar{\ell} \ell] + (F_P + \cos \theta F_{T5}) [\bar{\ell} \gamma_5 \ell] \right), \end{aligned} \tag{3.35}$$

where θ is the angle between ℓ^- and the flight direction of \bar{B} in the dilepton rest frame.

The F_i functions are defined as [60]

$$\begin{aligned} F_V(q^2) &= (C_9 + Y(q^2) + C_9') f_+(q^2) \\ &\quad + \frac{2m_b}{M_B + M_K} \left(C_7^{\text{eff}} + C_7' + \frac{4m_\ell}{m_b} C_T \right) f_T(q^2), \end{aligned} \tag{3.36}$$

$$F_A(q^2) = (C_{10} + C_{10}') f_+(q^2), \tag{3.37}$$

$$F_S(q^2) = \frac{M_B^2 - M_K^2}{2(m_b - m_s)} (C_S + C_S') f_0(q^2), \tag{3.38}$$

$$\begin{aligned} F_P(q^2) &= \frac{M_B^2 - M_K^2}{2(m_b - m_s)} (C_P + C_P') f_0(q^2) \\ &\quad - m_\ell (C_{10} + C_{10}') \\ &\quad \times \left[f_+(q^2) - \frac{M_B^2 - M_K^2}{q^2} (f_0(q^2) - f_+(q^2)) \right], \end{aligned} \tag{3.39}$$

$$F_T(q^2) = \frac{2\sqrt{\lambda} \beta_\ell}{M_B + M_K} C_T f_T(q^2), \tag{3.40}$$

$$F_{T5}(q^2) = \frac{2\sqrt{\lambda} \beta_\ell}{M_B + M_K} C_{T5} f_T(q^2). \tag{3.41}$$

where C_T and C_{T5} are tensor Wilson coefficients, which we take to be equal to zero in our analysis, and f_0, f_+, f_-, f_T are form factors. We consider the LCSR + lattice results from [61] together with their uncertainties and correlations.

F_V receives corrections from hadronic terms:

$$\delta F_V = \frac{2m_b}{M_B + M_K} \mathcal{T}_P, \tag{3.42}$$

where \mathcal{T}_P is given in [59,62].

To evaluate the uncertainties due to higher-order corrections, we again use the parameterisation

$$F_i \rightarrow F_i \left[1 + a_i + b_i \left(\frac{q^2}{6 \text{ GeV}^2/c^4} \right) \right], \tag{3.43}$$

with a_i and b_i uncorrelated complex nuisance parameters. As for the $B_d \rightarrow K^{*0} \mu^+ \mu^-$ angular observables, following the prescription of [41], we model the distributions of their

amplitudes as Gaussians centered at 0, with respective variances of 10% and 25% in the low- q^2 region, and 10% and 0% in the high- q^2 region, and take their phases to be uniformly random.

The decay rate is then given by

$$\Gamma(B \rightarrow K \ell^+ \ell^-) = 2 \left(A_\ell + \frac{1}{3} C_\ell \right), \tag{3.44}$$

where

$$A_\ell = \int_{q_{\min}^2}^{q_{\max}^2} dq^2 a_\ell(q^2), \quad C_\ell = \int_{q_{\min}^2}^{q_{\max}^2} dq^2 c_\ell(q^2). \tag{3.45}$$

with

$$a_\ell(q^2) = \mathcal{C}(q^2) \left[q^2 \left(\beta_\ell^2 |F_S|^2 + |F_P|^2 \right) + \frac{\lambda}{4} \left(|F_A|^2 + |F_V|^2 \right) \right. \tag{3.46}$$

$$\left. + 2m_\ell \left(M_B^2 - M_K^2 + q^2 \right) \times \text{Re}(F_P F_A^*) + 4m_\ell^2 M_B^2 |F_A|^2 \right],$$

$$c_\ell(q^2) = \mathcal{C}(q^2) \left[q^2 \left(\beta_\ell^2 |F_T|^2 + |F_{TS}|^2 \right) - \frac{\lambda}{4} \beta_\ell^2 \left(|F_A|^2 + |F_V|^2 \right) + 2m_\ell \sqrt{\lambda} \beta_\ell \text{Re}(F_T F_V^*) \right], \tag{3.47}$$

where $\lambda = \lambda(M_B^2, M_K^2, q^2)$ is as defined in Eq. (3.9),

$$\mathcal{C}(q^2) = \Gamma_0 \beta_\ell \sqrt{\lambda}, \tag{3.48}$$

with

$$\Gamma_0 = \frac{G_F^2 \alpha_e^2 |V_{tb} V_{ts}^*|^2}{512 \pi^5 M_B^3}. \tag{3.49}$$

3.4 Branching fraction of $B_s/B_d \rightarrow \mu^+ \mu^-$ decays

The rare decay $B_s \rightarrow \mu^+ \mu^-$ is strongly helicity-suppressed in the SM and proceeds via Z^0 penguin and box diagrams, but can receive large contributions from BSM physics. The main contribution to this decay is from the effective operator O_{10} in the SM and from the scalar and pseudoscalar operators $O_{S,P}$ in some BSM scenarios. As O_{10} has no contamination from four-quark operators, the generalisation to B_d decay is straightforward.

The branching fraction is given by

$$\text{BR}(B_s \rightarrow \mu^+ \mu^-) = \frac{G_F^2 \alpha^2}{64 \pi^3} f_{B_s}^2 \tau_{B_s} m_{B_s}^3 |V_{tb} V_{ts}^*|^2 \sqrt{1 - \frac{4m_\mu^2}{m_{B_s}^2}}$$

$$\times \left[\left(1 - \frac{4m_\mu^2}{m_{B_s}^2} \right) \left| \left(\frac{m_{B_s}}{m_b + m_s} \right) C_S \right|^2 + \left| \left(\frac{m_{B_s}}{m_b + m_s} \right) C_P + 2 C_{10} \frac{m_\mu}{m_{B_s}} \right|^2 \right], \tag{3.50}$$

where f_{B_s} is the B_s decay constant, m_{B_s} is the B_s meson mass and τ_{B_s} is the B_s mean life. As we consider only scenarios where new physics enters through modifications of C_7 , C_9 and/or C_{10} , in our analysis we set $C_S = C_P = 0$.

The main theoretical uncertainty comes from f_{B_s} , which is determined with lattice QCD. We use $f_{B_s} = 227.7$ MeV [63]. The main parametric uncertainty is from the CKM matrix element V_{ts} .

Within the minimal flavour violation approximation, the $B_d \rightarrow \ell^+ \ell^-$ rate can be obtained from the $B_s \rightarrow \ell^+ \ell^-$ rate simply by exchanging $s \rightarrow d$ in the above formula.

3.5 Branching fraction of inclusive $b \rightarrow s \gamma$ decays

Last but not least of the relevant processes in our study is the inclusive branching fraction of $b \rightarrow s \gamma$. As an inclusive decay, it does not suffer from form factor uncertainties, and it therefore provides the strongest constraint on the C_7 Wilson coefficient.

The branching fraction of $B \rightarrow X_s \gamma$ for a photon energy cut $E_\gamma > E_0$ is given by [64–70]

$$\text{BR}(B \rightarrow X_s \gamma)_{E_\gamma > E_0} = \text{BR}(B \rightarrow X_c e \bar{\nu})_{\text{exp}} \times \frac{6 \alpha_{\text{em}}}{\pi C} \left| \frac{V_{ts}^* V_{tb}}{V_{cb}} \right|^2 \left[P(E_0) + N(E_0) \right], \tag{3.51}$$

where $\alpha_{\text{em}} = \alpha_{\text{em}}^{\text{on shell}}$ [71], $C = |V_{ub}|^2 / |V_{cb}|^2 \times \Gamma[B \rightarrow X_c e \bar{\nu}] / \Gamma[B \rightarrow X_u e \bar{\nu}]$ and $P(E_0)$ and $N(E_0)$ denote the perturbative and nonperturbative contributions, respectively. We adopt the standard experimental cut $E_0 = 1.6$ GeV.

The perturbative contributions are known at NNLO precision, while the nonperturbative corrections are estimated to be below 5% [72]. The main sources of theoretical uncertainty are nonperturbative, parametric and perturbative (scale) uncertainties, and ambiguity arising from interpolation between results computed at different values of m_c .

The perturbative part of the Wilson coefficients is parameterised as

$$P(E_0) = P^{(0)}(\mu_b) + \left(\frac{\alpha_s(\mu_b)}{4\pi} \right) \left[P_1^{(1)}(\mu_b) + P_2^{(1)}(E_0, \mu_b) \right] + \mathcal{O}(\alpha_s^2(\mu_b)), \tag{3.52}$$

where bracketed superscripts indicate order in perturbation theory, and

$$P^{(0)}(\mu_b) = \left[C_7^{(0)\text{eff}}(\mu_b) \right]^2,$$

$$\begin{aligned}
 P_1^{(1)}(\mu_b) &= 2 C_7^{(0)\text{eff}}(\mu_b) C_7^{(1)\text{eff}}(\mu_b), \\
 P_2^{(1)}(E_0, \mu_b) &= \sum_{i,j=1}^8 C_i^{(0)\text{eff}}(\mu_b) C_j^{(0)\text{eff}}(\mu_b) K_{ij}^{(1)}(E_0, \mu_b).
 \end{aligned}
 \tag{3.53}$$

The functions $K_{ij}^{(1)}$ can be found in Ref. [67], $C_i^{\text{eff}}(\mu) = C_i(\mu)$ for $i = 1, \dots, 6$, $C_7^{\text{eff}}(\mu)$ is given in Eq. (3.10), and

$$C_8^{\text{eff}} = C_8(\mu) + C_3(\mu) - \frac{1}{6}C_4(\mu) + 20C_5(\mu) - \frac{10}{3}C_6(\mu).
 \tag{3.54}$$

We also consider the branching fraction for $B \rightarrow K^{*0}\gamma$ in the fit, following the theory calculation in Ref. [62].

3.6 Other measurements

Other potentially interesting experimental measurements of $b \rightarrow s\mu^+\mu^-$ decays are provided by observations of the decays of the Λ_b baryon, such as $\Lambda_b \rightarrow \Lambda\mu\mu$. The LHCb collaboration has measured both the branching fraction [73] and the angular distribution [74] using the method of moments [75, 76]. We have not considered these measurements here as they have much larger uncertainties than those of the corresponding meson decays. It is worth pointing out, however, that the Λ baryon is stable under strong interactions and therefore the computation of the form factors does not require a complicated treatment of multi-hadron states. Once more experimental data are available, recent [77] and future developments of lattice calculations mean that this decay will eventually be placed on the same footing as other $b \rightarrow s\mu^+\mu^-$ transitions.

In the current analysis, we only consider the lepton-universal Wilson coefficients. Therefore, we do not include any of the observables explicitly designed to test violation of lepton flavour universality, such as R_K or R_{K^*} . We defer the study of Wilson coefficients that violate lepton universality to future work.

4 Statistical treatment

We carry out global fits varying three Wilson coefficients: $\text{Re}(\Delta C_7)$, $\text{Re}(\Delta C_9)$ and $\text{Re}(\Delta C_{10})$. For each set of the three parameters, we compute the theoretical prediction for all considered observables and the covariance matrix corresponding to the uncertainties on the theoretical predictions arising from the variation of all theory nuisance parameters. We perform the fit using GAMBIT [32, 33], an open-source, modular package that combines theory calculations, experimental likelihoods, statistics and sampling routines. In particular, we use the FlavBit module [31] for computing all theoretical predictions and experimental likelihoods. The latest version

of FlavBit obtains observables via an interface to SuperIso 4.1 [34–36], and likelihoods via an interface to the HEPLike package [78], which retrieves experimental results and their correlated uncertainties from the HEPLikeData repository [79].

Here we present only profile likelihood results, which we obtain via the interface in the GAMBIT ScannerBit module to the differential evolution sampler Diver [80], run with a population of 20,000 and a convergence threshold parameter of 10^{-5} . We also carried out an equivalent Bayesian analysis using the ensemble Markov Chain Monte Carlo sampler T-Walk [80]; the results are practically identical to the profile likelihood ones, so we do not show them here.

To compute the theoretical covariance matrix, we follow a similar approach as the one described in [81]. Let us consider two observables Q and T , which are subject to elementary sources of uncertainties, numbered $a = (1, \dots, n)$. We denote the variations of the nuisance parameters as δ_a , which have an impact on both observables. Assuming that the uncertainties are small enough to affect the observables linearly, the total variation of observable Q is given at first order by:

$$Q = Q_0 \left(1 + \sum_{a=1}^n \delta_a \Delta_Q^a \right),
 \tag{4.1}$$

where Δ_Q^a is the relative variance generated by the nuisance parameter a and Q_0 is the central value. We denote the covariance matrix between the nuisance parameters as

$$\rho_{ab} = \text{Cov}[\delta_a, \delta_b].
 \tag{4.2}$$

such that the total relative variance of observable Q is

$$(\Delta_Q)^2 = \sum_{a,b} \rho_{ab} \Delta_Q^a \Delta_Q^b,
 \tag{4.3}$$

the correlation coefficient between Q and T is

$$(\Delta_{QT})^2 = \sum_{a,b} \rho_{ab} \Delta_Q^a \Delta_T^b,
 \tag{4.4}$$

and the covariance matrix of observables Q and T is therefore

$$\text{Cov}[Q, T] = \begin{pmatrix} (\Delta_Q)^2(Q_0)^2 & (\Delta_{QT})^2 Q_0 T_0 \\ (\Delta_{QT})^2 Q_0 T_0 & (\Delta_T)^2(T_0)^2 \end{pmatrix}.
 \tag{4.5}$$

In practice, most of the nuisance parameters are uncorrelated, so that $\rho_{ab} = \delta_{ab}$. The form factors on the other hand are strongly correlated, and we make sure to include their correlation matrices when computing Eq. 4.5.

In the following subsection we will discuss specifics of our treatment of different experimental likelihoods.

4.1 Angular distribution of $B_d \rightarrow K^{*0} \mu^+ \mu^-$, $B_d \rightarrow K^{*0} e^+ e^-$ and $B_u \rightarrow K^{*0} \mu^+ \mu^-$ decays

The angular coefficients of $B_d \rightarrow K^{*0} \mu^+ \mu^-$, $B_d \rightarrow K^{*0} e^+ e^-$ and $B_u \rightarrow K^{*0} \mu^+ \mu^-$ decays are measured by several experiments, using different methods and providing different information.

In the most recent LHCb publication [48], the angular observables are provided in bins of q^2 with the full experimental covariance matrix. In contrast to previous LHCb results [82], the uncertainties provided are symmetric, which is a consequence of increased statistics. The constructed experimental likelihood has the form:

$$\ln \mathcal{L}(C_i) = -\frac{1}{2} V^T(C_i) \text{Cov}^{-1}(C_i) V(C_i), \tag{4.6}$$

where \uparrow denotes the likelihood, Cov is the covariance matrix, and V is the vector of differences between the measured values and the theory predictions for a given set of Wilson coefficients (C_i).

In the case of other analyses [7, 83, 84],¹ the uncertainties are reported as asymmetric. In this case, we construct an experimental covariance matrix for each point depending on which of the asymmetric errors is relevant:

$$\text{Cov}[Q, T] = \begin{cases} \text{Corr}[Q, T] \sigma_+^Q \sigma_+^T, & \text{if } Q \geq Q_{obs} \text{ and } T \geq T_{obs} \\ \text{Corr}[Q, T] \sigma_+^Q \sigma_-^T, & \text{if } Q \geq Q_{obs} \text{ and } T < T_{obs} \\ \text{Corr}[Q, T] \sigma_-^Q \sigma_+^T, & \text{if } Q < Q_{obs} \text{ and } T \geq T_{obs} \\ \text{Corr}[Q, T] \sigma_-^Q \sigma_-^T, & \text{if } Q < Q_{obs} \text{ and } T < T_{obs}, \end{cases} \tag{4.7}$$

where σ_+^k , and σ_-^k are the reported asymmetric uncertainties of the k th observable, which we take to be given by the sum in quadrature of the reported systematic and statistical uncertainties. This is a refined treatment compared to some previous studies.

We then compute the total covariance matrix as the sum of the experimental and theoretical covariance matrices: $\text{Cov} = \text{Cov}_{\text{exp}} + \text{Cov}_{\text{th}}$.

4.2 Branching fractions of the $B_u \rightarrow K^{*0} \mu^+ \mu^-$, $B_d \rightarrow K^{*0} \mu^+ \mu^-$, $B_s \rightarrow \phi \mu^+ \mu^-$ and $B \rightarrow K \mu^+ \mu^-$ decays

In addition to the angular observables, we also include likelihoods for the branching fractions of $B_u \rightarrow K^{*0} \mu^+ \mu^-$, $B_d \rightarrow K^{*0} \mu^+ \mu^-$, $B_s \rightarrow \phi \mu^+ \mu^-$ and $B \rightarrow K \mu^+ \mu^-$ decays

in our fit, in multiple q^2 bins. Currently only the LHCb collaboration has measured these observables [52, 53, 56], with asymmetric uncertainties. We construct the likelihood in the same manner as in Sect. 4.1. The branching fractions of these decays are independent measurements and are statistically dominated. Therefore, no experimental correlation occurs between them. As for the $B_d \rightarrow K^{*0} \mu^+ \mu^-$ angular observables, we take into account asymmetric uncertainties.

4.3 Branching fractions of the $B_s \rightarrow \mu^+ \mu^-$ and $B_d \rightarrow \mu^+ \mu^-$ decays

The branching fractions of $B_s \rightarrow \mu^+ \mu^-$ and $B_d \rightarrow \mu^+ \mu^-$ have both been measured by LHCb [85], CMS [86] and ATLAS [87]. All these measurements were simultaneous determinations of both the B_d and B_s modes. All three publications provide two-dimensional log-likelihood information, which we use to construct our likelihoods.

For each two-dimensional set of measurements, we profile over a two-dimensional Gaussian distribution \mathcal{N} for the theoretical uncertainties on the branching ratios for $B_s \rightarrow \mu^+ \mu^-$ and $B_d \rightarrow \mu^+ \mu^-$, giving a final likelihood

$$\mathcal{L}(\text{BR}_s, \text{BR}_d) = \min_{\text{BR}'_s, \text{BR}'_d} \mathcal{L}_{\text{exp}}(\text{BR}'_s, \text{BR}'_d) \times \mathcal{N}(\text{BR}'_s, \text{BR}'_d | \text{BR}_s, \text{BR}_d, \text{Cov}), \tag{4.8}$$

where \mathcal{L}_{exp} is the two-dimensional experimental likelihood, BR_s and BR_d are the theoretically-predicted branching fractions of $B_s \rightarrow \mu^+ \mu^-$ and $B_d \rightarrow \mu^+ \mu^-$ decays respectively, while Cov is the covariance matrix describing their correlated uncertainties.

As all three experimental results have similar sensitivities, we include all three in our total likelihood function.

4.4 Inclusive branching fraction for $b \rightarrow s \gamma$ decays and exclusive branching fraction for $B \rightarrow K^{*0} \gamma$ and $B \rightarrow K^{*0} e^+ e^-$

We employ simple one-dimensional Gaussian likelihood based on the experimental measurement $\text{BR}(b \rightarrow s \gamma) = (3.32 \pm 0.15) \times 10^{-4}$, as recommended by the HFLAV collaboration [88]. This value is based on a photon energy requirement of $E_\gamma > 1.6$ GeV.

We do the same for $B \rightarrow K^{*0} \gamma$, constructing a one-dimensional Gaussian likelihood based on the HFLAV recommendation: $\text{BR}(B \rightarrow K^{*0} \gamma) = (4.1 \pm 0.12) \times 10^{-5}$ [88].

The decay $B \rightarrow K^{*0} e^+ e^-$ was measured by the LHCb Collaboration [89] in the low q^2 region of $q^2 \in [0.0008, 0.257]$ GeV². The signal in this region is dominated by the contribution from the radiative electroweak penguin diagram, constraining C_7 . The measurement consists of four

¹ In the case of the Belle experiment, we use the average between the muon and the electron mode.

Table 1 Results of the combined fit to the $\text{Re}(\Delta C_7)$, $\text{Re}(\Delta C_9)$, $\text{Re}(\Delta C_{10})$ Wilson coefficients. For each Wilson coefficient we give the best-fit value and the 1, 2 and 3σ intervals

Wilson coefficient	Best-fit point	68.3% interval	95.4% interval	99.7% interval
$\text{Re}(\Delta C_7)$	-0.011	[-0.004, 0.025]	[-0.018, 0.038]	[-0.032, 0.050]
$\text{Re}(\Delta C_9)$	-1.090	[-1.25, -0.93]	[-1.39, -0.77]	[-1.52, -0.61]
$\text{Re}(\Delta C_{10})$	-0.060	[-0.09, 0.17]	[-0.22, 0.29]	[-0.34, 0.41]

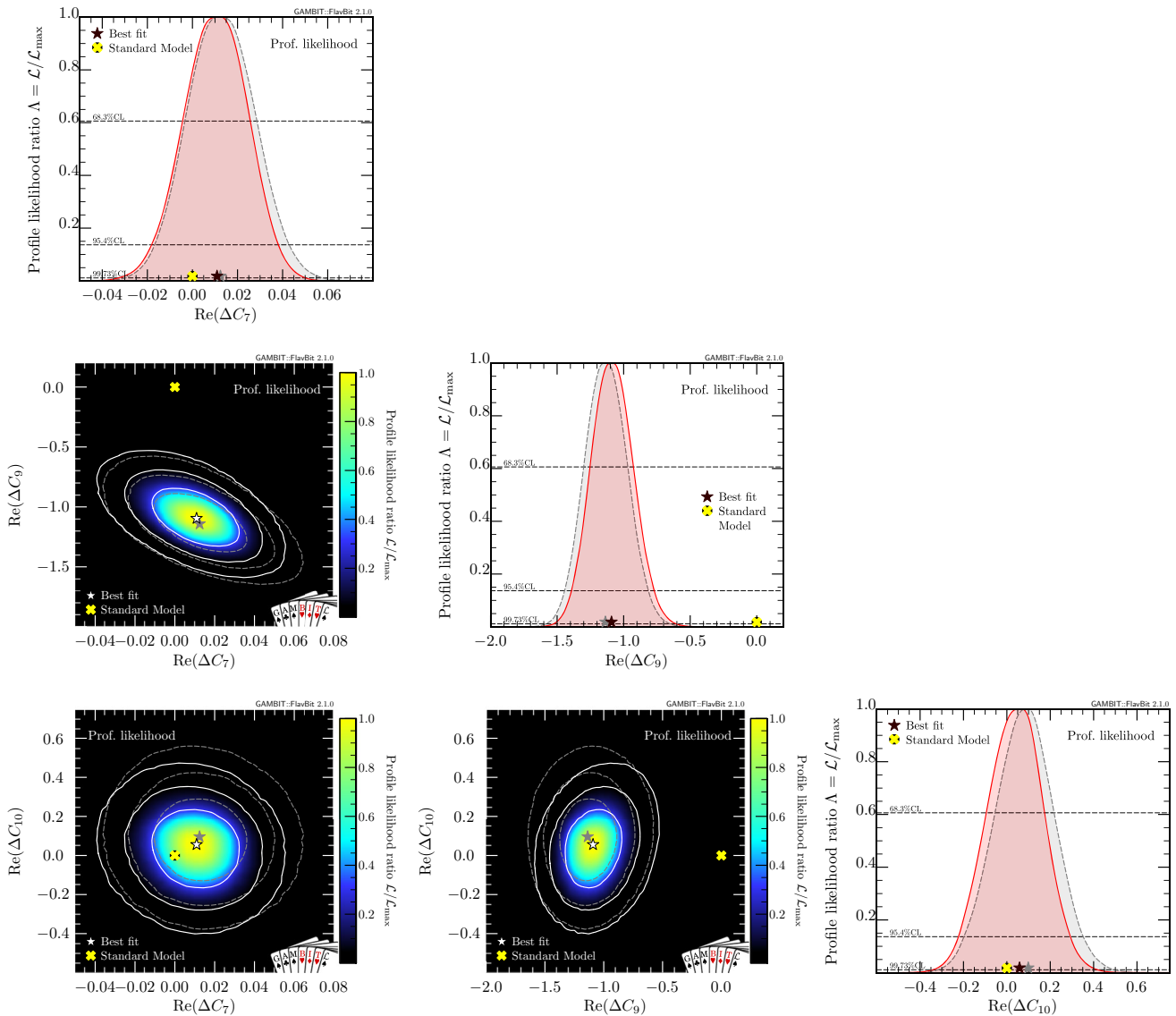


Fig. 1 Complete results of the combined fit to the $\text{Re}(\Delta C_7)$, $\text{Re}(\Delta C_9)$ and $\text{Re}(\Delta C_{10})$ Wilson coefficients, showing one- and two-dimensional profile likelihoods of each parameter. Contour lines indicate 1, 2 and 3σ confidence regions. White contours and coloured shading in two-dimensional planes, and red one-dimensional curves, show our main results, where we compute theory covariances self-

consistently for every combination of Wilson coefficients. Grey contours and curves show the corresponding result when we approximate the theory covariance by its value in the Standard Model, across the entire parameter space. The Standard Model prediction is indicated by a yellow cross

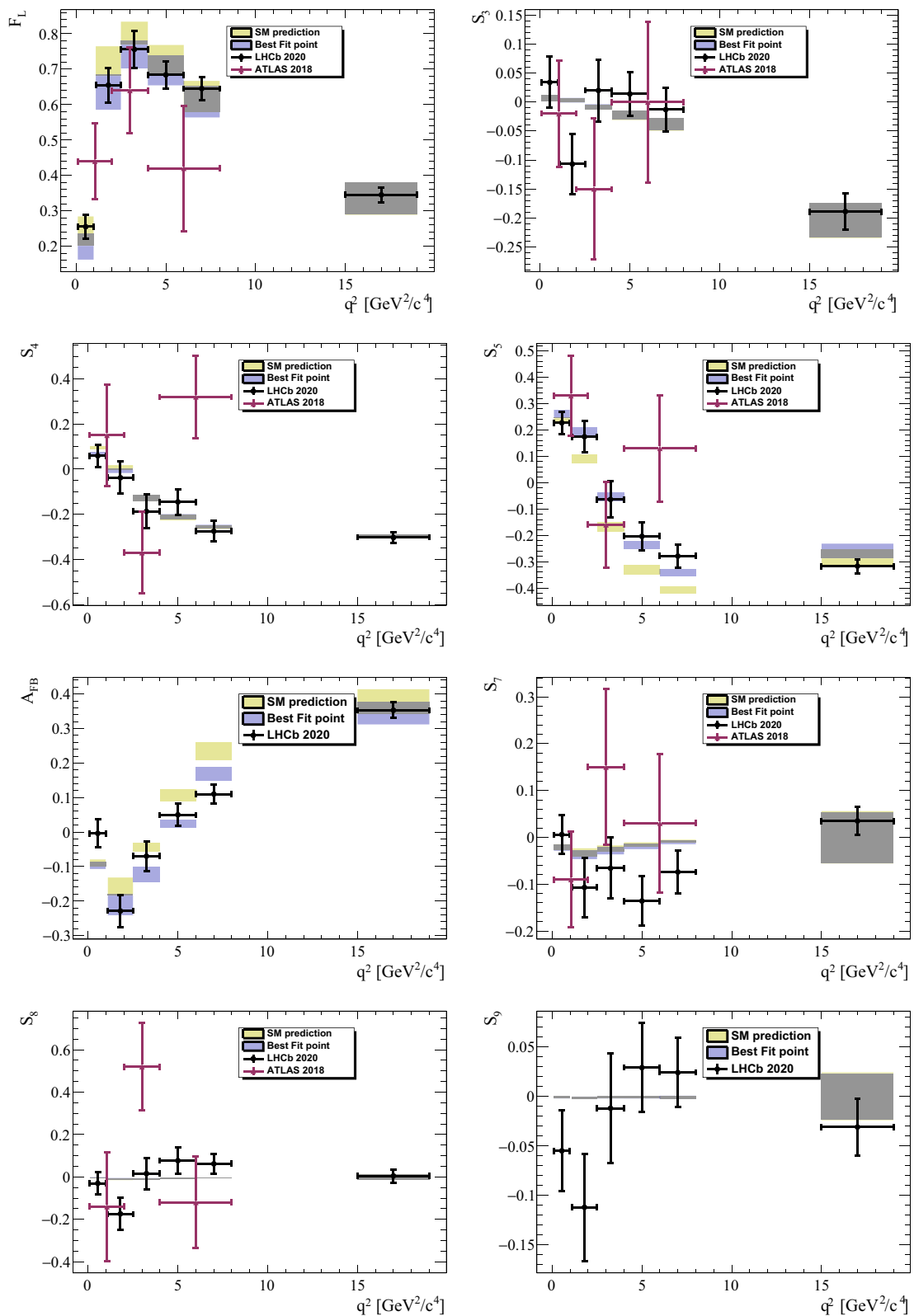


Fig. 2 Angular observables for the decay $B_d \rightarrow K^{*0} \mu^+ \mu^-$ included in our fit. Yellow shading corresponds to Standard Model predictions and uncertainties, and blue shading shows the prediction of our best-fit model. Data points with error bars show measurements from LHCb [48]

and ATLAS [8]. For display purposes, we present theoretical predictions using the same binning as LHCb; in the likelihood function, we always compare experimental results to theory predictions computed in the same binning as used by the experiment in question

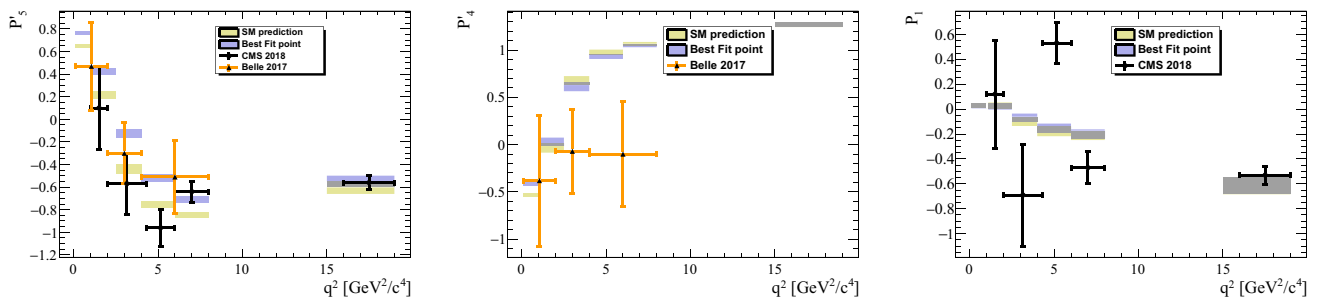


Fig. 3 Optimised angular observables for the decay $B_d \rightarrow K^{*0} \mu^+ \mu^-$ included in our fit. Yellow shading corresponds to Standard Model predictions and uncertainties, and blue shading shows the prediction of our best-fit model. Data points with error bars show measurements from Belle [50] and CMS [83]. For display purposes, we

amplitudes provided with correlations, from which we construct a four-dimensional likelihood function.

5 Results

5.1 Current status

In Table 1 and Fig. 1 we present the main results of our global fit, providing one and two dimensional profile likelihoods for each of the Wilson coefficients. As can be seen, the strongest required modification to the SM Wilson coefficients is in $\text{Re}(C_9)$. The best-fit points correspond to coupling strengths $\text{Re}(C_7)/\text{Re}(C_7^{\text{SM}}) = 0.96$, $\text{Re}(C_9)/\text{Re}(C_9^{\text{SM}}) = 0.74$, and $\text{Re}(C_{10})/\text{Re}(C_{10}^{\text{SM}}) = 0.99$ relative to the SM. The agreement with the SM can be quantified by comparing the log-likelihood of the best-fit point to that of the SM. This gives a total of $\Delta \ln \mathcal{L} = 25.8$, which for the three degrees of freedom in our fit, corresponds to a 6.6σ exclusion of the SM. Considering just $\text{Re}(C_9)$ alone, i.e. also profiling out the impacts of allowing $\text{Re}(C_7)$ and $\text{Re}(C_{10})$ to vary, such that only a single degree of freedom remains, we find $\Delta \ln \mathcal{L} = 19.6$. This corresponds to a 6.3σ preference for a non-SM value of C_9 .²

Previous analysis of older datasets in terms of the same Wilson coefficients have assumed that the covariance matrix describing the theoretical uncertainties on the observable predictions could be reliably approximated by its value com-

puted for the SM, across the entire Wilson coefficient parameter space. In our fits, we have explicitly recomputed these theoretical uncertainties at every point in the Wilson coefficient parameter space. We show the impact of this improvement in Fig. 1, by indicating with a grey star and dashed grey curves the best fit and 1, 2 and 3σ confidence regions that would result from adopting the SM approximation. The central value is not strongly affected, but the impact upon the resulting confidence regions is non-negligible.

In Figs. 2, 3, 4 and 5, we provide plots of the key observables and data that enter our fit. These consist of the $B_d \rightarrow K^{*0} \mu^+ \mu^-$ angular observables in the S_i basis (Fig. 2), their optimised versions (Fig. 3), branching fractions for other $b \rightarrow s$ processes (Fig. 4), and the joint measurement of the branching fractions of $B_s \rightarrow \mu^+ \mu^-$ and $B_d \rightarrow \mu^+ \mu^-$ (Fig. 5). We show the predictions of both the SM and our best-fit point, the theoretical uncertainties in each case, and the respective data from LHCb, ATLAS, CMS and Belle used in our fits. The improvement offered by the best-fit point is most visible in the S_5 and A_{FB} angular observables (Fig. 2), and in the overall branching fractions for $B_d \rightarrow K^{*0} \mu^+ \mu^-$ and $B_s \rightarrow \phi \mu^+ \mu^-$ decays (Fig. 4). Some reduction is expected in the branching fractions for $b \rightarrow s \gamma$ and $B \rightarrow K^{*0} \gamma$ relative to the SM in our best-fit model (Fig. 4), owing to the small positive best-fit value of $\text{Re}(C_7)$ (recalling that the SM value of C_7 is negative). These are however sufficiently small that the predictions remain consistent with the HFLAV value [88].

In Figs. 2, 3, 4 and 5, we provide plots of the key observables and data that enter our fit. These consist of the $B_d \rightarrow K^{*0} \mu^+ \mu^-$ angular observables in the S_i basis (Fig. 2), their optimised versions (Fig. 3), branching fractions for other $b \rightarrow s$ processes (Fig. 4), and the joint measurement of the branching fractions of $B_s \rightarrow \mu^+ \mu^-$ and $B_d \rightarrow \mu^+ \mu^-$ (Fig. 5). We show the predictions of both the SM and our best-fit point, the theoretical uncertainties in each case, and the respective data from LHCb, ATLAS, CMS and Belle used in our fits. The improvement offered by the best-fit point is most visible in the S_5 and A_{FB} angular observables (Fig. 2), and in the overall branching fractions for $B_d \rightarrow K^{*0} \mu^+ \mu^-$ and $B_s \rightarrow \phi \mu^+ \mu^-$ decays (Fig. 4). Some reduction is expected in the branching fractions for $b \rightarrow s \gamma$ and $B \rightarrow K^{*0} \gamma$ relative to the SM in our best-fit model (Fig. 4), owing to the small positive best-fit value of $\text{Re}(C_7)$ (recalling that the SM value of C_7 is negative). These are however sufficiently small that the predictions remain consistent with the HFLAV value [88].

5.2 Implications for future searches

With higher precision measurements of $B_d \rightarrow K^{*0} \mu^+ \mu^-$ in the future, Wilson coefficient fits will of course increase in precision. There are however also ongoing efforts to extract the non-factorisable contributions directly from $B_d \rightarrow K^{*0} \mu^+ \mu^-$ data [90]. The Belle II experiment has recently started taking data as well, with the aim of eventually reach-

² These calculations assume that the asymptotic limit of Wilks' theorem holds, i.e. that in the asymptotic limit of a large data sample, twice the difference $\Delta \ln \mathcal{L}$ follows a χ^2 distribution with n degrees of freedom, where n is the difference in dimensionality between the larger parameter space (the Wilson coefficient model + nuisances) and the nested one (the SM, with 0 free parameters + nuisances). For the 3-parameter fit $n = 3$, and for the C_9 -only test, $n = 1$. Given that our best fit lies far from the edges of the parameter space and the overall sample size is large, assuming the asymptotic limit of Wilks' theorem is a very good approximation under the assumption of normally-distributed errors.

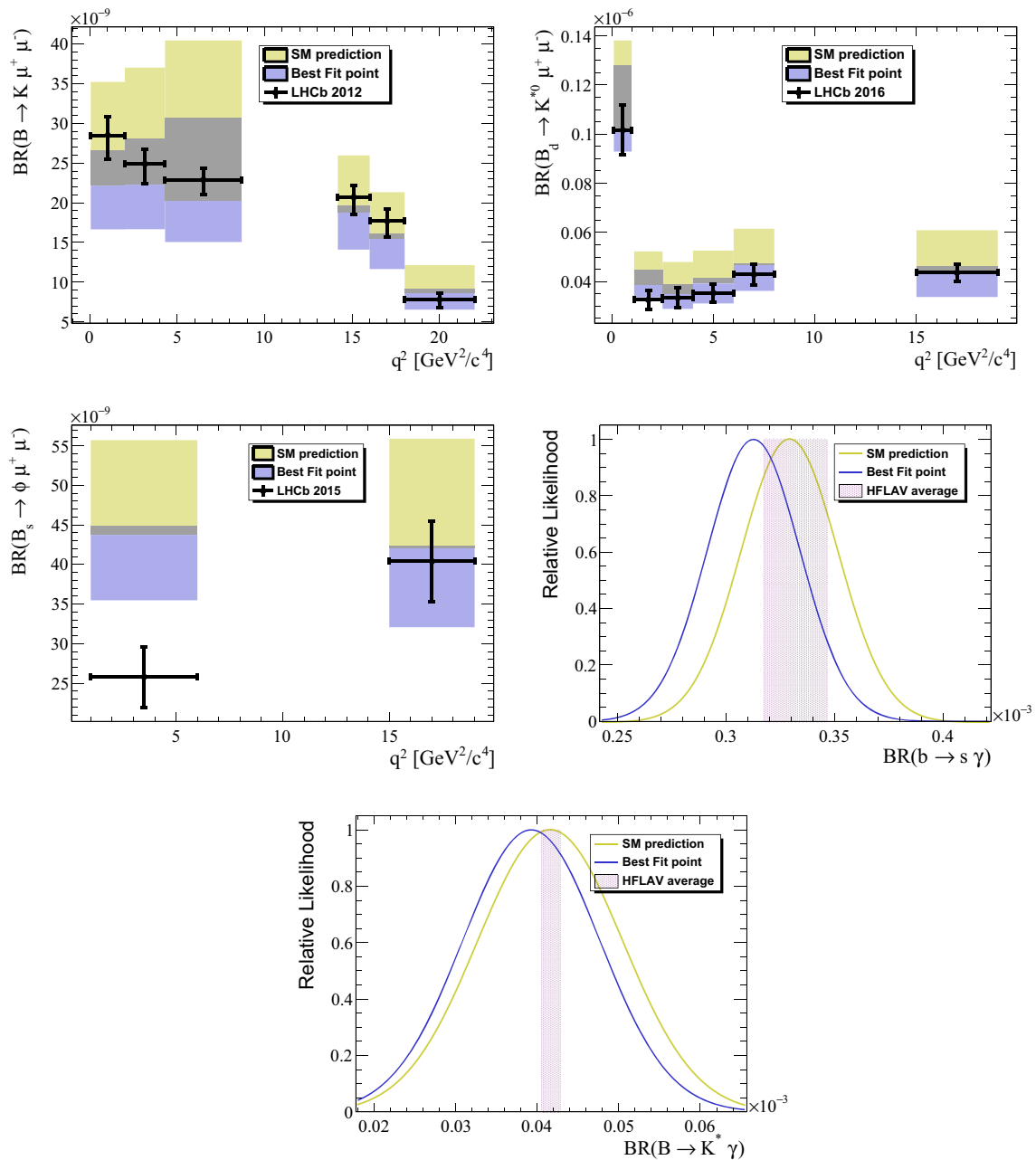


Fig. 4 Branching fractions for $b \rightarrow s$ transitions included in our fit. Yellow shading corresponds to Standard Model predictions and uncertainties, and blue shading shows the prediction of our best-fit model. Data

points with error bars show measurements from LHCb [52,53,56]. The $b \rightarrow s \gamma$ and $B \rightarrow K^{*0} \gamma$ measurements are taken from HFLAV [88]

ing 50 ab^{-1} integrated luminosity. The unprecedented number of decays that will be contained in this dataset creates the possibility to measure the branching fraction for inclusive $B \rightarrow X_{\mu}^{+} \mu^{-}$ decays. In Fig. 6, we show the predictions for $BR(B \rightarrow X_{\mu}^{+} \mu^{-})$ in our best-fit model and in the SM, for two example q^2 ranges. We overlay an expected Belle II measurement, with the central value set to our best-fit prediction and the uncertainty band based on the predicted sensitivity of Ref. [91]. Belle II will clearly have sufficient sensitivity

in the low- q^2 region to strongly distinguish the best-fit point from the SM.

6 Conclusions

We have used the FlavBit module of the GAMBIT package to perform a simultaneous fit of the real parts of the Wilson coefficients C_7 , C_9 and C_{10} , using combined data on

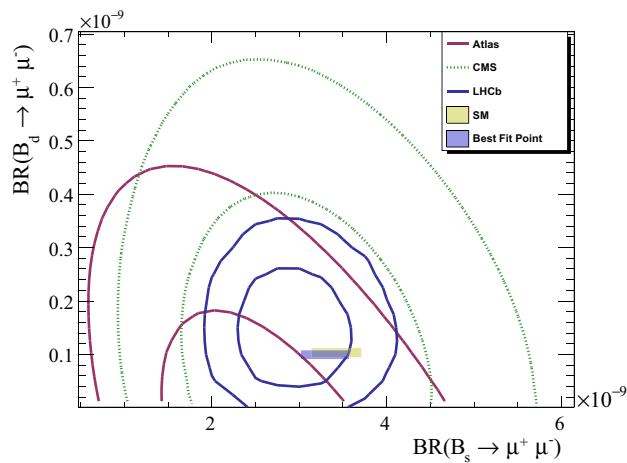


Fig. 5 Branching fractions for $B_s/B_d \rightarrow \mu^+\mu^-$ decays included in our fit. Contour lines correspond to the joint 1 and 2σ confidence regions obtained in the measurements by ATLAS [87], CMS [86] and LHCb [85]. Yellow shading corresponds to Standard Model predictions and uncertainties, and blue shading shows the prediction and uncertainty of our best-fit model

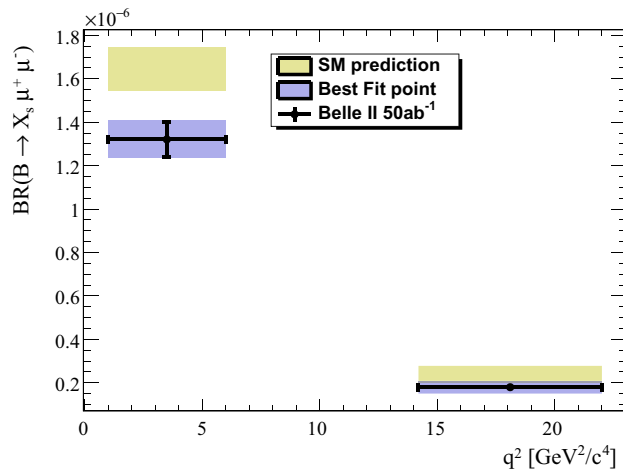


Fig. 6 Predicted exclusive branching fraction $BR(B \rightarrow X\mu^+\mu^-)$ in the Standard model (yellow shading) and in our best-fit model (blue shading). We also show the expected sensitivity of Belle II after it has collected 50 ab^{-1} of data [91], assuming that the central measured values are equal to our best-fit prediction

$b \rightarrow s\mu^+\mu^-$ transitions. Our results show that measurements of flavour anomalies in this sector have reached an intriguing historical juncture, as they are now sufficiently persistent that their tension with the SM increases steadily as new data are collected. With the inclusion of recently updated results from the LHCb collaboration, we find best-fit values relative to the SM predictions of $\text{Re}(C_7)/\text{Re}(C_7^{\text{SM}}) = 0.96$, $\text{Re}(C_9)/\text{Re}(C_9^{\text{SM}}) = 0.74$, and $\text{Re}(C_{10})/\text{Re}(C_{10}^{\text{SM}}) = 0.99$. Performing a hypothesis test of the SM by comparing the log-likelihood of our best-fit point to that of the SM, we obtain a 6.6σ preference for our best-fit point over the SM. This reduces slightly to 6.3σ when C_7 and C_{10} are profiled out.

By explicitly recomputing the theoretical uncertainty covariance matrix at every point in the Wilson coefficient parameter space, we have shown that the best-fit value is not strongly affected by departing from the usual assumption of an SM-only calculation, but that the effect is important for correctly determining confidence intervals, and therefore the overall significance of the result. Our results still rely on our specific choice of parameterisation of the non-factorisable QCD corrections to many key observables, but the more accurate treatment that we employ of the theory uncertainties across the Wilson coefficient parameter space is an important step forward in improving the test of the SM hypothesis.

Inspection of the observables that entered our fit indicate that our best-fit point better matches measurements of the S_5 and A_{FB} observables than the SM, in addition to the overall branching fractions for $B_d \rightarrow K^{*0}\mu^+\mu^-$ and $B_s \rightarrow \phi\mu^+\mu^-$ decays. Other observables are less strongly affected. Localisation of the apparent new physics contribution in a shift of the C_9 Wilson coefficient means that the physics should result from a vector coupling of b and s quarks to muons.

Acknowledgements MC and JB are supported by the Polish National Agency for Academic Exchange under the Bekker program, MC by The Foundation for Polish Science (FNP), PS by the Australian Research Council under grant FT190100814 and MJW by the Australian Research Council Discovery Project DP180102209. This research was supported in part by PL-Grid Infrastructure. We also acknowledge PRACE for awarding us access to Marconi at CINECA, Italy, and Joliot-Curie at CEA, France. MC is grateful for the hospitality of the Institute of Advanced Study, TUM. Figure 1 was produced with `pippi` [92].

Data Availability Statement This manuscript has no associated data or the data will not be deposited. [Authors' comment: The data is available now on Zenodo: <https://zenodo.org/record/5749788#.YajPYpHMKIs>.]

Open Access This article is licensed under a Creative Commons Attribution 4.0 International License, which permits use, sharing, adaptation, distribution and reproduction in any medium or format, as long as you give appropriate credit to the original author(s) and the source, provide a link to the Creative Commons licence, and indicate if changes were made. The images or other third party material in this article are included in the article's Creative Commons licence, unless indicated otherwise in a credit line to the material. If material is not included in the article's Creative Commons licence and your intended use is not permitted by statutory regulation or exceeds the permitted use, you will need to obtain permission directly from the copyright holder. To view a copy of this licence, visit <http://creativecommons.org/licenses/by/4.0/>.
Funded by SCOAP³.

References

1. S.L. Glashow, J. Iliopoulos, L. Maiani, Weak interactions with lepton-hadron symmetry. *Phys. Rev. D* **2**, 1285 (1970). <https://doi.org/10.1103/PhysRevD.2.1285>
2. LHCb Collaboration, R. Aaij et al., Measurement of Form-Factor-Independent Observables in the Decay $B^0 \rightarrow K^{*0}\mu^+\mu^-$.

- Phys. Rev. Lett.* **111**, 191801 (2013). <https://doi.org/10.1103/PhysRevLett.111.191801>. arXiv:1308.1707
3. LHCb Collaboration, R. Aaij et al., Differential branching fraction and angular analysis of the decay $B_s^0 \rightarrow \phi\mu^+\mu^-$. *JHEP* **07**, 084 (2013). [https://doi.org/10.1007/JHEP07\(2013\)084](https://doi.org/10.1007/JHEP07(2013)084). arXiv:1305.2168
 4. LHCb, R. Aaij et al., Branching fraction measurements of the rare $B_s^0 \rightarrow \phi\mu^+\mu^-$ and $B_s^0 \rightarrow f_2'(1525)\mu^+\mu^-$ decays. arXiv:2105.14007
 5. LHCb Collaboration, R. Aaij et al., Measurement of the phase difference between short- and long-distance amplitudes in the $B^+ \rightarrow K^+\mu^+\mu^-$ decay. *Eur. Phys. J. C* **77**, 161 (2017). <https://doi.org/10.1140/epjc/s10052-017-4703-2>. arXiv:1612.06764
 6. LHCb Collaboration, R. Aaij et al., Differential branching fraction and angular analysis of $\Lambda_b^0 \rightarrow \Lambda\mu^+\mu^-$ decays. *JHEP* **06**, 115 (2015). arXiv:1503.07138 [Erratum: *JHEP* **09**, 145 (2018)]
 7. Belle Collaboration, R. Aaij et al., Angular analysis of $B^0 \rightarrow K^*(892)^0\ell^+\ell^-$, in *A First Discussion of 13 TeV Results: Oberurgel, Austria, April 10–15, 2016* (2016). arXiv:1604.04042
 8. ATLAS Collaborations, R. Aaij et al., Angular analysis of $B_d^0 \rightarrow K^*\mu^+\mu^-$ decays in pp collisions at $\sqrt{s} = 8$ TeV with the ATLAS detector. *JHEP* **10**, 047 (2018). [https://doi.org/10.1007/JHEP10\(2018\)047](https://doi.org/10.1007/JHEP10(2018)047). arXiv:1805.04000
 9. CMS Collaboration, R. Aaij et al., Measurement of angular parameters from the decay $B^0 \rightarrow K^{*0}\mu^+\mu^-$ in proton-proton collisions at $\sqrt{s} = 8$ TeV. *Phys. Lett. B* **781**, 517 (2018). <https://doi.org/10.1016/j.physletb.2018.04.030>. arXiv:1710.02846
 10. G. D'Amico, M. Nardecchia, P. Panci, F. Sannino, A. Strumia, R. Torre et al., Flavour anomalies after the R_{K^*} measurement. *JHEP* **09**, 010 (2017). [https://doi.org/10.1007/JHEP09\(2017\)010](https://doi.org/10.1007/JHEP09(2017)010). arXiv:1704.05438
 11. L.-S. Geng, B. Grinstein, S. Jäger, J. MartinCamalich, X.-L. Ren, R.-X. Shi, Towards the discovery of new physics with lepton-universality ratios of $b \rightarrow s\ell\ell$ decays. *Phys. Rev. D* **96**(2017). <https://doi.org/10.1103/PhysRevD.96.093006>. arXiv:1704.05446
 12. T. Hurth, F. Mahmoudi, D. Martinez Santos, S. Neshatpour, Lepton nonuniversality in exclusive $b \rightarrow s\ell\ell$ decays. *Phys. Rev. D* **96**, 095034 (2017). <https://doi.org/10.1103/PhysRevD.96.095034>. arXiv:1705.06274
 13. M. Algueró, B. Capdevila, A. Crivellin, S. Descotes-Genon, P. Masjuan, J. Matias et al., Emerging patterns of new physics with and without lepton flavour universal contributions. *Eur. Phys. J. C* **79**, 714 (2019). <https://doi.org/10.1140/epjc/s10052-019-7216-3>. arXiv:1903.09578
 14. A.K. Alok, A. Dighe, S. Gangal, D. Kumar, Continuing search for new physics in $b \rightarrow s\mu\mu$ decays: two operators at a time. *JHEP* **06**, 089 (2019). [https://doi.org/10.1007/JHEP06\(2019\)089](https://doi.org/10.1007/JHEP06(2019)089). arXiv:1903.09617
 15. M. Ciuchini, A.M. Coutinho, M. Fedele, E. Franco, A. Paul, L. Silvestrini et al., New physics in $b \rightarrow s\ell^+\ell^-$ confronts new data on lepton universality. *Eur. Phys. J. C* **79**, 719 (2019). <https://doi.org/10.1140/epjc/s10052-019-7210-9>. arXiv:1903.09632
 16. J. Aebischer, W. Altmannshofer, D. Guadagnoli, M. Reboud, P. Stangl, D.M. Straub, B-decay discrepancies after Moriond 2019. *Eur. Phys. J. C* **80**, 252 (2020). <https://doi.org/10.1140/epjc/s10052-020-7817-x>. arXiv:1903.10434
 17. K. Kowalska, D. Kumar, E.M. Sessolo, Implications for new physics in $b \rightarrow s\mu\mu$ transitions after recent measurements by Belle and LHCb. *Eur. Phys. J. C* **79**, 840 (2019). <https://doi.org/10.1140/epjc/s10052-019-7330-2>. arXiv:1903.10932
 18. A. Arbey, T. Hurth, F. Mahmoudi, S. Neshatpour, Hadronic and new physics contributions to $b \rightarrow s$ transitions. *Phys. Rev. D* **98**, 095027 (2018). <https://doi.org/10.1103/PhysRevD.98.095027>. arXiv:1806.02791
 19. A. Datta, J. Kumar, D. London, The B anomalies and new physics in $b \rightarrow se^+e^-$. *Phys. Lett. B* **797**, 134858 (2019). <https://doi.org/10.1016/j.physletb.2019.134858>. arXiv:1903.10086
 20. A. Arbey, T. Hurth, F. Mahmoudi, D.M. Santos, S. Neshatpour, Update on the $b \rightarrow s$ anomalies. *Phys. Rev. D* **100**, 015045 (2019). <https://doi.org/10.1103/PhysRevD.100.015045>. arXiv:1904.08399
 21. A. Khodjamirian, T. Mannel, A. Pivovarov, Y.-M. Wang, Charm-loop effect in $B \rightarrow K^{(*)}\ell^+\ell^-$ and $B \rightarrow K^*\gamma$. *JHEP* **09**, 089 (2010). [https://doi.org/10.1007/JHEP09\(2010\)089](https://doi.org/10.1007/JHEP09(2010)089). arXiv:1006.4945
 22. A. Khodjamirian, T. Mannel, Y. Wang, $B \rightarrow K\ell^+\ell^-$ decay at large hadronic recoil. *JHEP* **02**, 010 (2013). [https://doi.org/10.1007/JHEP02\(2013\)010](https://doi.org/10.1007/JHEP02(2013)010). arXiv:1211.0234
 23. M. Dimou, J. Lyon, R. Zwicky, Exclusive chromomagnetism in heavy-to-light FCNCs. *Phys. Rev. D* **87**, 074008 (2013). <https://doi.org/10.1103/PhysRevD.87.074008>. arXiv:1212.2242
 24. J. Lyon, R. Zwicky, Isospin asymmetries in $B \rightarrow (K^*, \rho)\gamma/l^+l^-$ and $B \rightarrow Kl^+l^-$ in and beyond the standard model. *Phys. Rev. D* **88**, 094004 (2013). <https://doi.org/10.1103/PhysRevD.88.094004>. arXiv:1305.4797
 25. J. Lyon, R. Zwicky, Resonances gone topsy turvy—the charm of QCD or new physics in $b \rightarrow s\ell^+\ell^-$? arXiv:1406.0566
 26. C. Bobeth, M. Chruszcz, D. van Dyk, J. Virto, Long-distance effects in $B \rightarrow K^*\ell\ell$ from analyticity. *Eur. Phys. J. C* **78**, 451 (2018). <https://doi.org/10.1140/epjc/s10052-018-5918-6>. arXiv:1707.07305
 27. T. Blake, U. Egede, P. Owen, K.A. Petridis, G. Pomery, An empirical model to determine the hadronic resonance contributions to $\bar{B}^0 \rightarrow \bar{K}^{*0}\mu^+\mu^-$ transitions. *Eur. Phys. J. C* **78**, 453 (2018). <https://doi.org/10.1140/epjc/s10052-018-5937-3>. arXiv:1709.03921
 28. T. Hurth, F. Mahmoudi, S. Neshatpour, On the new LHCb angular analysis of $B \rightarrow K^*\mu^+\mu^-$: hadronic effects or new physics? *Phys. Rev. D* **102**, 055001 (2020). <https://doi.org/10.1103/PhysRevD.102.055001>. arXiv:2006.04213
 29. LHCb Collaboration, *Test of lepton universality in beauty-quark decays*. arXiv:2103.11769
 30. LHCb Collaboration, R. Aaij et al., Test of lepton universality with $B^0 \rightarrow K^{*0}\ell^+\ell^-$ decays. *JHEP* **08**, 055 (2017). [https://doi.org/10.1007/JHEP08\(2017\)055](https://doi.org/10.1007/JHEP08(2017)055). arXiv:1705.05802
 31. The GAMBIT Flavour Workgroup, *FlavBit: a GAMBIT module for computing flavour observables and likelihoods*. *Eur. Phys. J. C* **77**, 786 (2017). <https://doi.org/10.1140/epjc/s10052-017-5157-2>. arXiv:1705.07933
 32. GAMBIT Collaboration, P. Athron et al., GAMBIT: the global and modular beyond-the-standard-model inference tool. *Eur. Phys. J. C* **77**, 784 (2017). arXiv:1705.07908 [Addendum: *Eur. Phys. J. C* **78**, 98 (2018)]
 33. A. Kvellestad, P. Scott, M. White, GAMBIT and its application in the search for physics beyond the standard model. *Prog. Part. Nuc. Phys.* (2020). arXiv:1912.04079
 34. F. Mahmoudi, SuperIso: a program for calculating the isospin asymmetry of $B \rightarrow K^*\gamma$ in the MSSM. *Comput. Phys. Commun.* **178**, 745 (2008). <https://doi.org/10.1016/j.cpc.2007.12.006>. arXiv:0710.2067
 35. F. Mahmoudi, SuperIso v2.3: a program for calculating flavor physics observables in Supersymmetry. *Comput. Phys. Commun.* **180**, 1579 (2009). <https://doi.org/10.1016/j.cpc.2009.02.017>. arXiv:0808.3144
 36. F. Mahmoudi, SuperIso v3.0, flavor physics observables calculations: extension to NMSSM. *Comput. Phys. Commun.* **180**, 1718 (2009). <https://doi.org/10.1016/j.cpc.2009.05.001>
 37. U. Egede, T. Hurth, J. Matias, M. Ramon, W. Reece, New observables in the decay mode $\bar{B}_d \rightarrow \bar{K}^{*0}l^+l^-$. *JHEP*

- 11, 032 (2008). <https://doi.org/10.1088/1126-6708/2008/11/032>. [arXiv:0807.2589](https://arxiv.org/abs/0807.2589)
38. U. Egede, T. Hurth, J. Matias, M. Ramon, W. Reece, New physics reach of the decay mode $\bar{B} \rightarrow \bar{K}^{*0} \ell^+ \ell^-$. *JHEP* **10**, 056 (2010). [https://doi.org/10.1007/JHEP10\(2010\)056](https://doi.org/10.1007/JHEP10(2010)056). [arXiv:1005.0571](https://arxiv.org/abs/1005.0571)
39. A. Bharucha, D.M. Straub, R. Zwicky, $B \rightarrow V \ell^+ \ell^-$ in the Standard Model from light-cone sum rules. *JHEP* **08**, 098 (2016). [https://doi.org/10.1007/JHEP08\(2016\)098](https://doi.org/10.1007/JHEP08(2016)098). [arXiv:1503.05534](https://arxiv.org/abs/1503.05534)
40. M. Beneke, T. Feldmann, D. Seidel, Exclusive radiative and electroweak $b \rightarrow d$ and $b \rightarrow s$ penguin decays at NLO. *Eur. Phys. J. C* **41**, 173 (2005). <https://doi.org/10.1140/epjc/s2005-02181-5>. [arXiv:hep-ph/0412400](https://arxiv.org/abs/hep-ph/0412400)
41. T. Hurth, F. Mahmoudi, S. Neshatpour, On the anomalies in the latest LHCb data. *Nucl. Phys. B* **909**, 737 (2016). <https://doi.org/10.1016/j.nuclphysb.2016.05.022>. [arXiv:1603.00865](https://arxiv.org/abs/1603.00865)
42. V. Chobanova, T. Hurth, F. Mahmoudi, D. MartinezSantos, S. Neshatpour, Large hadronic power corrections or new physics in the rare decay $B \rightarrow K^* \mu^+ \mu^-$? *JHEP* **07**, 025 (2017). [https://doi.org/10.1007/JHEP07\(2017\)025](https://doi.org/10.1007/JHEP07(2017)025). [arXiv:1702.02234](https://arxiv.org/abs/1702.02234)
43. J. Matias, F. Mescia, M. Ramon, J. Virto, Complete Anatomy of $\bar{B}_d \rightarrow \bar{K}^{*0} (\rightarrow K\pi) l^+ l^-$ and its angular distribution. *JHEP* **04**, 104 (2012). [https://doi.org/10.1007/JHEP04\(2012\)104](https://doi.org/10.1007/JHEP04(2012)104). [arXiv:1202.4266](https://arxiv.org/abs/1202.4266)
44. S. Descotes-Genon, T. Hurth, J. Matias, J. Virto, Optimizing the basis of $B \rightarrow K^* l l$ observables in the full kinematic range. *JHEP* **05**, 137 (2013). [https://doi.org/10.1007/JHEP05\(2013\)137](https://doi.org/10.1007/JHEP05(2013)137). [arXiv:1303.5794](https://arxiv.org/abs/1303.5794)
45. R. Sinha, CP violation in B mesons using Dalitz plot asymmetries. [arXiv:hep-ph/9608314](https://arxiv.org/abs/hep-ph/9608314)
46. F. Kruger, L. M. Sehgal, N. Sinha, R. Sinha, Angular distribution and CP asymmetries in the decays $\bar{B} \rightarrow K^- \pi^+ e^- e^+$ and $\bar{B} \rightarrow \pi^- \pi^+ e^- e^+$. *Phys. Rev. D* **61**, 114028 (2000). [arXiv:hep-ph/9907386](https://arxiv.org/abs/hep-ph/9907386) [Erratum: *Phys. Rev. D* **63**, 019901 (2001)]
47. W. Altmannshofer, P. Ball, A. Bharucha, A.J. Buras, D.M. Straub, M. Wick, Symmetries and asymmetries of $B \rightarrow K^* \mu^+ \mu^-$ decays in the standard model and beyond. *JHEP* **01**, 019 (2009). <https://doi.org/10.1088/1126-6708/2009/01/019>. [arXiv:0811.1214](https://arxiv.org/abs/0811.1214)
48. LHCb Collaboration, Measurement of CP-averaged observables in the $B^0 \rightarrow K^{*0} \mu^+ \mu^-$ decay. [arXiv:2003.04831](https://arxiv.org/abs/2003.04831)
49. J. Gratrex, M. Hopfer, R. Zwicky, Generalised helicity formalism, higher moments and the $B \rightarrow K_{JK} (\rightarrow K\pi) \bar{\ell}_1 \ell_2$ angular distributions. *Phys. Rev. D* **93**, 054008 (2016). <https://doi.org/10.1103/PhysRevD.93.054008>. [arXiv:1506.03970](https://arxiv.org/abs/1506.03970)
50. Belle Collaboration, S. Wehle et al., Lepton-flavor-dependent angular analysis of $B \rightarrow K^* \ell^+ \ell^-$. *Phys. Rev. Lett.* **118**, 111801 (2017). <https://doi.org/10.1103/PhysRevLett.118.111801>. [arXiv:1612.05014](https://arxiv.org/abs/1612.05014)
51. LHCb Collaboration, R. Aaij et al., Differential branching fraction and angular analysis of the decay $B^0 \rightarrow K^{*0} \mu^+ \mu^-$. *JHEP* **08**, 131 (2013). [https://doi.org/10.1007/JHEP08\(2013\)131](https://doi.org/10.1007/JHEP08(2013)131). [arXiv:1304.6325](https://arxiv.org/abs/1304.6325)
52. LHCb Collaboration, R. Aaij et al., Measurements of the S-wave fraction in $B^0 \rightarrow K^+ \pi^- \mu^+ \mu^-$ decays and the $B^0 \rightarrow K^{*0} \mu^+ \mu^-$ differential branching fraction. *JHEP* **11**, 047 (2016). [arXiv:1606.0473](https://arxiv.org/abs/1606.0473) [Erratum: *JHEP* **04**, 142 (2017)]
53. LHCb Collaboration, R. Aaij et al., Angular analysis and differential branching fraction of the decay $B_s^0 \rightarrow \phi \mu^+ \mu^-$. *JHEP* **09**, 179 (2015). [https://doi.org/10.1007/JHEP09\(2015\)179](https://doi.org/10.1007/JHEP09(2015)179). [arXiv:1506.08777](https://arxiv.org/abs/1506.08777)
54. S. Descotes-Genon, J. Virto, Time dependence in $B \rightarrow V \ell \ell$ decays. *JHEP* **04**, 045 (2015). [https://doi.org/10.1007/JHEP04\(2015\)045](https://doi.org/10.1007/JHEP04(2015)045). [arXiv:1502.05509](https://arxiv.org/abs/1502.05509)
55. Particle Data Group, M. Tanabashi et al., Review of particle physics. *Phys. Rev. D* **98**, 030001 (2018). <https://doi.org/10.1103/PhysRevD.98.030001>
56. LHCb, R. Aaij et al., Differential branching fraction and angular analysis of the $B^+ \rightarrow K^+ \mu^+ \mu^-$ decay. *JHEP* **02**, 105 (2013). [https://doi.org/10.1007/JHEP02\(2013\)105](https://doi.org/10.1007/JHEP02(2013)105). [arXiv:1209.4284](https://arxiv.org/abs/1209.4284)
57. BaBar, B. Aubert et al., Direct CP, lepton flavor and isospin asymmetries in the decays $B \rightarrow K^{(*)} \ell^+ \ell^-$. *Phys. Rev. Lett.* **102**, 091803 (2009). <https://doi.org/10.1103/PhysRevLett.102.091803>. [arXiv:0807.4119](https://arxiv.org/abs/0807.4119)
58. Belle, J.-T. Wei et al., Measurement of the Differential Branching Fraction and Forward-Backward Asymmetry for $B \rightarrow K^{(*)} \ell^+ \ell^-$. *Phys. Rev. Lett.* **103**, 171801 (2009). <https://doi.org/10.1103/PhysRevLett.103.171801>. [arXiv:0904.0770](https://arxiv.org/abs/0904.0770)
59. C. Bobeth, G. Hiller, G. Piranishvili, Angular distributions of $\bar{B} \rightarrow \bar{K} \ell^+ \ell^-$ decays. *JHEP* **12**, 040 (2007). <https://doi.org/10.1088/1126-6708/2007/12/040>. [arXiv:0709.4174](https://arxiv.org/abs/0709.4174)
60. D. Becirevic, N. Kosnik, F. Mescia, E. Schneider, Complementarity of the constraints on new physics from $B_s \rightarrow \mu^+ \mu^-$ and from $B \rightarrow K l^+ l^-$ decays. *Phys. Rev. D* **86**, 034034 (2012). <https://doi.org/10.1103/PhysRevD.86.034034>. [arXiv:1205.5811](https://arxiv.org/abs/1205.5811)
61. W. Altmannshofer, D.M. Straub, New physics in $b \rightarrow s$ transitions after LHC run I. *Eur. Phys. J. C* **75**, 382 (2015). <https://doi.org/10.1140/epjc/s10052-015-3602-7>. [arXiv:1411.3161](https://arxiv.org/abs/1411.3161)
62. M. Beneke, T. Feldmann, D. Seidel, Systematic approach to exclusive $B \rightarrow V l^+ l^-, V \gamma$ decays. *Nucl. Phys. B* **612**, 25 (2001). [https://doi.org/10.1016/S0550-3213\(01\)00366-2](https://doi.org/10.1016/S0550-3213(01)00366-2). [arXiv:hep-ph/0106067](https://arxiv.org/abs/hep-ph/0106067)
63. Flavour Lattice Averaging Group, S. Aoki et al., FLAG Review 2019: Flavour Lattice Averaging Group (FLAG). *Eur. Phys. J. C* **80**, 113 (2020). <https://doi.org/10.1140/epjc/s10052-019-7354-7>. [arXiv:1902.08191](https://arxiv.org/abs/1902.08191)
64. R. Grigjanis, P.J. O'Donnell, M. Sutherland, H. Navelet, QCD corrected effective Lagrangian for $B \rightarrow s$ processes. *Phys. Lett. B* **213**, 355 (1988). [https://doi.org/10.1016/0370-2693\(88\)91774-1](https://doi.org/10.1016/0370-2693(88)91774-1)
65. B. Grinstein, R.P. Springer, M.B. Wise, Effective Hamiltonian for weak radiative B meson decay. *Phys. Lett. B* **202**, 138 (1988). [https://doi.org/10.1016/0370-2693\(88\)90868-4](https://doi.org/10.1016/0370-2693(88)90868-4)
66. M. Misiak et al., Estimate of $\mathcal{B}(\bar{B} \rightarrow X_s \gamma)$ at $O(\alpha_s^2)$. *Phys. Rev. Lett.* **98**, 022002 (2007). <https://doi.org/10.1103/PhysRevLett.98.022002>. [arXiv:hep-ph/0609232](https://arxiv.org/abs/hep-ph/0609232)
67. M. Misiak, M. Steinhauser, NNLO QCD corrections to the anti-B $\rightarrow X(s)$ gamma matrix elements using interpolation in $m(c)$. *Nucl. Phys. B* **764**, 62 (2007). <https://doi.org/10.1016/j.nuclphysb.2006.11.027>. [arXiv:hep-ph/0609241](https://arxiv.org/abs/hep-ph/0609241)
68. M. Czakon, P. Fiedler, T. Huber, M.A. Misiak, T. Schutzmeier, M. Steinhauser, The $(Q_7, Q_{1,2})$ contribution to $\bar{B} \rightarrow X_s \gamma$ at $O(\alpha_s^2)$. *JHEP* **04**, 168 (2015). [https://doi.org/10.1007/JHEP04\(2015\)168](https://doi.org/10.1007/JHEP04(2015)168). [arXiv:1503.01791](https://arxiv.org/abs/1503.01791)
69. M. Misiak, A. Rehman, M. Steinhauser, NNLO QCD counterterm contributions to $\bar{B} \rightarrow X_s \gamma$ for the physical value of m_c . *Phys. Lett. B* **770**, 431 (2017). <https://doi.org/10.1016/j.physletb.2017.05.008>. [arXiv:1702.07674](https://arxiv.org/abs/1702.07674)
70. M. Misiak, A. Rehman, M. Steinhauser, Towards $\bar{B} \rightarrow X_s \gamma$ at the NNLO in QCD without interpolation in m_c . [arXiv:2002.01548](https://arxiv.org/abs/2002.01548)
71. A. Czarnecki, W.J. Marciano, Electroweak radiative corrections to $b \rightarrow s$ gamma. *Phys. Rev. Lett.* **81**, 277 (1998). <https://doi.org/10.1103/PhysRevLett.81.277>. [arXiv:hep-ph/9804252](https://arxiv.org/abs/hep-ph/9804252)
72. A. Gunawardana, G. Paz, Reevaluating uncertainties in $\bar{B} \rightarrow X_s \gamma$ decay. *JHEP* **11**, 141 (2019). [https://doi.org/10.1007/JHEP11\(2019\)141](https://doi.org/10.1007/JHEP11(2019)141). [arXiv:1908.02812](https://arxiv.org/abs/1908.02812)
73. LHCb Collaboration, R. Aaij et al., Observation of the suppressed decay $\Lambda_b^0 \rightarrow p \pi^- \mu^+ \mu^-$. *JHEP* **04**, 029 (2017). [https://doi.org/10.1007/JHEP04\(2017\)029](https://doi.org/10.1007/JHEP04(2017)029). [arXiv:1701.08705](https://arxiv.org/abs/1701.08705)
74. LHCb Collaboration, R. Aaij et al., Angular moments of the decay $\Lambda_b^0 \rightarrow \Lambda \mu^+ \mu^-$ at low hadronic recoil. *JHEP* **09**, 146 (2018). [https://doi.org/10.1007/JHEP09\(2018\)146](https://doi.org/10.1007/JHEP09(2018)146). [arXiv:1808.00264](https://arxiv.org/abs/1808.00264)

75. T. Blake, M. Kreps, Angular distribution of polarised Λ_b baryons decaying to $\Lambda \ell^+ \ell^-$. *JHEP* **11**, 138 (2017). [https://doi.org/10.1007/JHEP11\(2017\)138](https://doi.org/10.1007/JHEP11(2017)138). [arXiv:1710.00746](https://arxiv.org/abs/1710.00746)
76. F. Beaujean, M. Chrzaszcz, N. Serra, D. van Dyk, Extracting angular observables without a likelihood and applications to rare decays. *Phys. Rev. D* **91**, 114012 (2015). <https://doi.org/10.1103/PhysRevD.91.114012>. [arXiv:1503.04100](https://arxiv.org/abs/1503.04100)
77. W. Detmold, S. Meinel, $\Lambda_b \rightarrow \Lambda \ell^+ \ell^-$ form factors, differential branching fraction, and angular observables from lattice QCD with relativistic b quarks. *Phys. Rev. D* **93**(2016). <https://doi.org/10.1103/PhysRevD.93.074501>. [arXiv:1602.01399](https://arxiv.org/abs/1602.01399)
78. J. Bhom, M. Chrzaszcz, HEPLike: an open source framework for experimental likelihood evaluation. *Comput. Phys. Commun.* (2020). <https://doi.org/10.1016/j.cpc.2020.107235>. [arXiv:2003.03956](https://arxiv.org/abs/2003.03956)
79. J. Bhom, M. Chrzaszcz, HEPLikeData, 2020. <https://www.github.com/mchrzaszcz/HEPLikeData>
80. GAMBIT Scanner Workgroup, G.D. Martinez, J. McKay, et al., Comparison of statistical sampling methods with ScannerBit, the GAMBIT scanning module. *Eur. Phys. J. C* **77**, 761 (2017) <https://doi.org/10.1140/epjc/s10052-017-5274-y>. [arXiv:1705.07959](https://arxiv.org/abs/1705.07959)
81. A. Arbey, S. Fichet, F. Mahmoudi, G. Moreau, The correlation matrix of Higgs rates at the LHC. *JHEP* **11**, 097 (2016). [https://doi.org/10.1007/JHEP11\(2016\)097](https://doi.org/10.1007/JHEP11(2016)097). [arXiv:1606.00455](https://arxiv.org/abs/1606.00455)
82. LHCb Collaboration, R. Aaij et al., Angular analysis of the $B^0 \rightarrow K^{*0} \mu^+ \mu^-$ decay using 3 fb^{-1} of integrated luminosity. *JHEP* **02**, 104 (2016). [https://doi.org/10.1007/JHEP02\(2016\)104](https://doi.org/10.1007/JHEP02(2016)104). [arXiv:1512.04442](https://arxiv.org/abs/1512.04442)
83. CMS Collaboration, Measurement of the P_1 and P'_5 angular parameters of the decay $B^0 \rightarrow K^{*0} \mu^+ \mu^-$ in proton–proton collisions at $\sqrt{s} = 8 \text{ TeV}$. Technical report CMS-PAS-BPH-15-008, CERN, Geneva (2017)
84. LHCb, R. Aaij et al., Angular analysis of the $B^+ \rightarrow K^{*+} \mu^+ \mu^-$ decay. *Phys. Rev. Lett.* **126**, 161802 (2021). <https://doi.org/10.1103/PhysRevLett.126.161802>. [arXiv:2012.13241](https://arxiv.org/abs/2012.13241)
85. LHCb Collaboration, R. Aaij et al., Measurement of the $B_s^0 \rightarrow \mu^+ \mu^-$ branching fraction and effective lifetime and search for $B^0 \rightarrow \mu^+ \mu^-$ decays. *Phys. Rev. Lett.* **118**, 191801 (2017). <https://doi.org/10.1103/PhysRevLett.118.191801>. [arXiv:1703.05747](https://arxiv.org/abs/1703.05747)
86. CMS Collaboration, Measurement of properties of B_s^0 to $\mu^+ \mu^-$ decays and search for B_0 to $\mu^+ \mu^-$ with the CMS experiment. Technical report CMS-PAS-BPH-16-004, CERN, Geneva (2019)
87. ATLAS Collaboration, M. Aaboud et al, Study of the rare decays of B_s^0 and B^0 mesons into muon pairs using data collected during 2015 and 2016 with the ATLAS detector. *JHEP* **04**, 098 (2019). [https://doi.org/10.1007/JHEP04\(2019\)098](https://doi.org/10.1007/JHEP04(2019)098). [arXiv:1812.03017](https://arxiv.org/abs/1812.03017)
88. HFLAV Collaboration, Y. Amhis et al., HFLAV input to the update of the European Strategy for Particle Physics. [arXiv:1812.07461](https://arxiv.org/abs/1812.07461)
89. LHCb, R. Aaij et al., Strong constraints on the $b \rightarrow s \gamma$ photon polarisation from $B^0 \rightarrow K^{*0} e^+ e^-$ decays. *JHEP* **12**, 081 (2020). [https://doi.org/10.1007/JHEP12\(2020\)081](https://doi.org/10.1007/JHEP12(2020)081). [arXiv:2010.06011](https://arxiv.org/abs/2010.06011)
90. A. Mauri, N. Serra, R. SilvaCoutinho, Towards establishing lepton flavor universality violation in $\bar{B} \rightarrow \bar{K}^* \ell^+ \ell^-$ decays. *Phys. Rev. D* **99**, 013007 (2019). <https://doi.org/10.1103/PhysRevD.99.013007>. [arXiv:1805.06401](https://arxiv.org/abs/1805.06401)
91. Belle-II, W. Altmannshofer et al., *The Belle II Physics Book*. *PTEP* **123C01** (2019). <https://doi.org/10.1093/ptep/ptz106>. [arXiv:1808.10567](https://arxiv.org/abs/1808.10567)
92. P. Scott, Pippi–painless parsing, post-processing and plotting of posterior and likelihood samples. *Eur. Phys. J. Plus* **127**, 138 (2012). [arXiv:1206.2245](https://arxiv.org/abs/1206.2245)